BINARY WAVEFRONT OPTIMIZATION FOR FOCUSING LIGHT THROUGH SCATTERING MEDIA

by

XIAOLONG ZHANG

(Under the Direction of Peter Kner)

ABSTRACT

Random light scattering in inhomogeneous media causes strong wavefront aberrations and makes it impossible to focus light. Many wavefront correction techniques have been recently demonstrated to control light propagation in these media. Phase modulation with a spatial light modulator (SLM) and digital light modulator (DMD) have been used to correct the aberrations. And real-time wavefront optimization algorithms have also been developed based on different techniques. In this study, we demonstrate two new techniques, using binary wavefront optimization to focus light through scattering media. We have developed a genetic algorithm and a transmission matrix algorithm for focusing light with binary wavefront optimization. We apply these methods to binary amplitude modulation with both a spatial light modulator and a digital light modulator. With the genetic algorithm, we achieve a focal spot 105 times stronger than the initial average intensity dividing the wavefront into 1024 segments, 64.5% of the theoretical maximum. With the transmission matrix algorithm, we used 6144 segments to achieve a focal spot enhancement of 532, 54.4% of the theoretical maximum.

INDEX WORDS: Wavefront Optimization, Scattering Media, Spatial light Modulator

BINARY WAVEFRONT OPTIMIZATION FOR FOCUSING LIGHT THROUGH SCATTERING MEDIA

by

XIAOLONG ZHANG

BS, Shandong University of Chinese Medicine, China, 2010

A Thesis Submitted to the Graduate Faculty of The University of Georgia in Partial Fulfillment of the Requirements for the Degree

MASTER OF SCIENCE

ATHENS, GEORGIA

2014

BINARY WAVEFRONT OPTIMIZATION FOR FOCUSING LIGHT THROUGH

SCATTERING MEDIA

by

XIAOLONG ZHANG

Major Professor: Peter A. Kner

Committee: Mark A. Haidekker
William S. Kisaalita

Electronic Version Approved:

Julie Coffield
Interim Dean of the Graduate School
The University of Georgia
August 2014

TABLE OF CONTENTS

LIST OF TABLES

LIST OF FIGURES

CHAPTER 1

INTRODUCTION AND LITERATURE REVIEW

1.1 Introduction

In turbid media, the scattering length is short compared to the thickness so that rays of light exiting the material have no relation to the rays that entered. Therefore, we cannot see through turbid media and light cannot be focused through it, Figure1.1. Researchers would like to control light propagation in order to achieve high resolution imaging through scattering materials. Brain is one example of a turbid media, and there is great research interest in imaging through the brain. The Brain Research through Advancing Innovative Neurotechnologies (BRAIN) Initiative, part of a new Presidential focus, seeks to generate a revolutionary new dynamic picture and understanding of the brain [1]. If light can be focused through turbid media, then scanning microscopy techniques such as confocal and multiphoton microscopy could be used to image an entire mouse brain, providing unprecedented opportunities for researchers to explore how the brain enables the human body to record, process, utilize, store, and retrieve vast quantities of information [1, 2].

Figure 1.1: Milk is an example of a strongly scattering material. Milk does not absorb light, but is still opaque [3].

Several techniques for wavefront correction have been developed to correct optical aberrations in imaging systems. Adaptive Optics (AO) with a deformable mirror (DM) or a liquid crystal spatial light modulator (LC-SLM) dramatically corrects wavefront aberrations, and AO is used not only in astronomy but also in biological imaging. Wavefront optimization algorithms are performed in phase only modulation with a SLM and binary amplitude modulation with a digital light processor (DMD). Previous researches on wavefront optimization are shown in section 1.2.

1.2 Literature Review

Recently it has been demonstrated that light can be focused through strongly scattering samples by controlling the phase of the input field in the back pupil [4]. This can be viewed as an extreme version of adaptive optics for propagation through distances many times the scattering length of the material. This work has generated considerable excitement because of the possibility of using this approach to optimize imaging through strongly scattering biological samples [2].

The Light beam in the back pupil can be divided into a number of segments by a wavefront modulator and the phase on each segment can be modulated. When the phase is set to the optimal value, a focus spot with high enhancement is created on the CCD target area. Enhancement is defined as the ratio of the average intensity before correction to the maximum intensity after correction. An illustration of phase modulation reported by Mosk is shown in Figure 1.2.

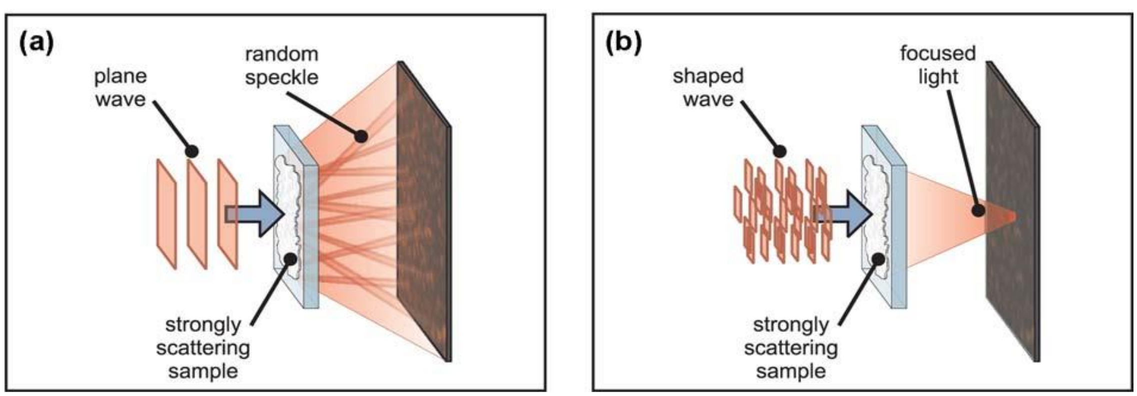

Figure 1.2: Theory of phase modulation. (a) Before optimization, a speckle pattern is achieved on CCD. (b) After correction, a sharp focus is achieved [4].

Many research groups have demonstrated methods for wavefront optimization using spatial light modulators (SLM), including sequential algorithms [5], parallel algorithms [6], and genetic algorithms [7]. The transfer matrix characterizing the sample can also be directly measured and then inverted to achieve focusing at single or multiple points [8]. SLMs operate at maximum rates of approximately 100Hz, and optimization of thousands of channels can take between a minute to several hours. For example, to optimize 3228 channels requires 4 measurements per channel and would take over two minutes at 100Hz.

To increase the speed of wavefront optimization, faster devices are needed. Digital Micromirror Device (DMD) can operate at rates up to 32 kHz, but DMDs are binary devices which can turn each pixel on or off but cannot directly adjust the pixel phase. DMDs can be used to focus light through random samples by only turning on the light rays that send light to the focal point; this is referred to as binary amplitude modulation [9]. For a device with N segments, this leads to an enhancement at the focal spot of $\sim N/2\pi$, a factor of $\pi^2/2$ smaller than the enhancement possible from phase modulation. Nevertheless, more channels can be optimized faster, so it should be possible to achieve higher enhancements.

DMDs have been used for phase modulation by using binary amplitude off-axis holography to generate a wavefront with arbitrary phase from a binary amplitude pattern [10]. The downside to this approach is that creating the off-axis hologram requires writing a grating with the DMD which limits the number of channels, N, that are used for focusing. This approach has been used with 256 segments. Although binary amplitude modulation results in a smaller theoretical enhancement, it can be used with many more channels, so can achieve an overall higher enhancement.

Binary amplitude modulation has been demonstrated with a sequential algorithm [9] and with a transfer matrix algorithm [11]. The transfer matrix approach requires measuring the phase and amplitude of the output with an interferometer. In both reports, the enhancement achieved using a DMD is substantially lower than $N/2\pi$. In [9], an enhancement of 19 is achieved compared to the expected value of 514 for N=3228. In [11], an enhancement of 343 is achieved compared to the expected value of 1592 for N=10,000.

In this study, we develop two new algorithms for rapid focusing in turbid media, a genetic algorithm and a transmission matrix algorithm for binary amplitude optimization. Genetic algorithms have been shown to work the best in media with shorter persistence times, and we show that the genetic algorithm performs better than sequential control algorithms for binary wavefront optimization. And the transmission matrix algorithm demonstrates an even better optimization than the genetic algorithm.

CHAPTER 2

LIGHT SCATTERING IN TURBID MEDIA

2.1 Introduction

Many media like paint, milk or biological tissue are non-transparent because the inhomogeneity of these media causes light scattering. Light scattering such as Mie scattering Rayleigh scattering, and Raman scattering is a type of scattering in which light is the form of scattered propagating energy. Rayleigh scattering is the elastic scattering of light or other electromagnetic radiation by particles whose size is much smaller than the wavelength of the light. When photons are scattering from an atom or molecule, most photons are elastically scattered, but a small fraction of the scattered photons are scattered by an excitation, with the scattered photons having a higher or lower frequency than the incident photons due to the exchange of energy with the vibrations of the atom or molecule; this is Raman scattering. Mie scattering describes the scattering of electromagnetic radiation by spherical particles whose size is similar to the wavelength of the light. Since latex beads, the fat particles in milk and biological cells and organelles are in this size range and roughly spherical, Mie scattering is an important approximation for these materials [12]. Light scattering can be considered as the deflection of light rays from the incoming parallel light, as shown in Figure 2.1.

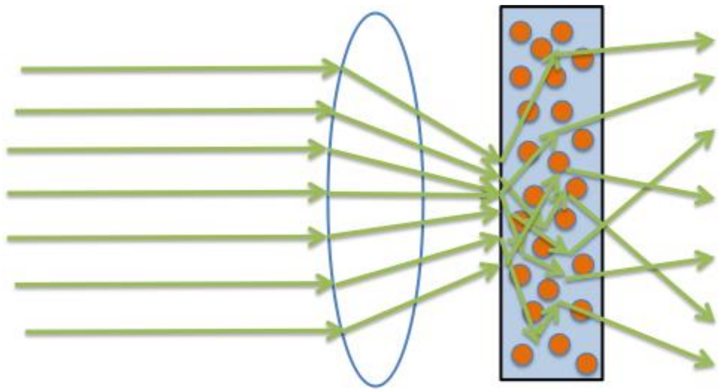

Figure 2.1: Light scattering in turbid media.

A collimated beam is attenuated in a thin tissue layer of thickness d in accordance with the Bouguer-Beer-Lambert exponential law [13],

$$I = (1 - R_F) I_0 e^{-\mu_t d} \tag{2.1}$$

where I is the intensity of transmitted light. R_F is the coefficient of Fresnel refraction. I_0 is the incident light intensity. μ_t is the extinction coefficient.

$$\mu_t = \mu_a + \mu_s \tag{2.2}$$

where μ_a is the absorption coefficient and μ_s is the scattering coefficient.

The turbid media only scatters light instead of absorbing light, so the absorption coefficient is close to zero and then $\mu_t = \mu_s$. The mean free path (MFP) between two interactions is defined by Equation 2.4 [13],

$$L_{ph} = {\mu_t}^{-1} = {\mu_s}^{-1} \tag{2.3}$$

The ratio of the sample thickness and scattering length is L_0/L_{ph}.

Different media have different persistence times T_p, and persistence time is defined as the time that the sample is maintaining stable during measurement, which is the decay time of the field autocorrelate of the transmitted speckle [5]. It is defined by Equation 2.4.

$$S = S_0 e^{-T/T_p} \tag{2.4}$$

S_0 is the initial speckle and S is the decayed speckle.

Light scattering and interference inside turbid media strongly distorts the wavefront and the coherent spatial information is scrambled. The scattering mean free path is short compared to the propagation distance. It seems that it is impossible to focus light through these media, but actually, scattering is deterministic so that the sample can be characterized by a transmission matrix. And light propagation can be still controlled by measuring the transmission matrix.

2.2 Transmission matrix model

The transmission matrix t_{mn} is straightforwardly described as the relationship between the incident wavefront and the transmitted one, as shown in Figure 2.2. The incident wavefront can be decomposed into a set of orthogonal modes, such as rays or Hermite-Gaussian modes [14]. The transmitted wavefront can also be decomposed into orthogonal modes so that the relationship between the output and input can be described by a matrix relating the complex amplitudes of the output modes to the input modes. The electric field on the *m*th output mode is defined as,

$$E_m = \sum_{n=1}^{N} t_{mn} A_n e^{i\varphi_n} \tag{2.5}$$

where A_n is the amplitude of the incident light and φ_n is the phase for the n^{th} input mode [4]. To completely describe the wavefront would require an infinite number of modes, but in practice a finite number can provide a good description of the wavefront.

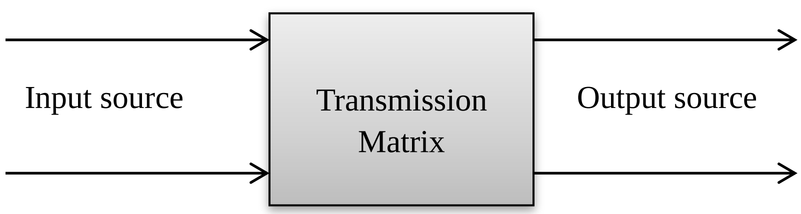

Figure 2.2: Concept of transmission matrix.

For ideal optical elements such as a lens, the TM is a 2×2 matrix operating on a vector describing the rays [15]. The height and angle of transmitted light can be determined by Equation 2.6,

$$\begin{bmatrix} h' \\ u' \end{bmatrix} = \begin{bmatrix} 1 & 0 \\ -f^{-1} & 1 \end{bmatrix} \begin{bmatrix} h \\ u \end{bmatrix} = \begin{bmatrix} h \\ u - h/f \end{bmatrix} \tag{2.6}$$

where h and u are the height and angle of the incident light and h' and u' are the height and angle of the transmitted light. f is the focal length of the ideal optical lens.

But for heterogeneous media such as paint, the wavefront is completely scrambled and almost none of the neighbors are the same, thus the TM must be a large matrix consisting of thousands of elements, as shown in Figure 2.3. In this case the TM input and output are all the modes (rays) that are coupled by the system.

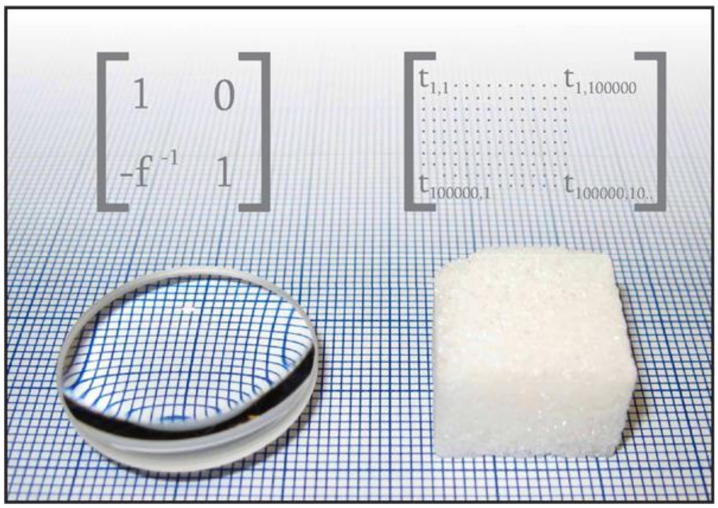

Figure 2.3: Transmission Matrix of ideal lens (Left) and turbid media (Right) [15].

For scattering media, the TM is a matrix of nonzero, complex Gaussian random values. It is a large matrix, Equation 2.7, instead of a 2×2 matrix for ideal lens. A good knowledge of the transmission matrix can help us to understand light transport inside the media so that we can easily control it to create a focal spot.

$$T = \begin{bmatrix} t_{1,1} & \cdots & \cdots & t_{1,n} \\ \vdots & \ddots & \ddots & \vdots \\ t_{m,1} & \ldots & \ldots & t_{m,n} \end{bmatrix} \tag{2.7}$$

Where $t_{i,j} = a + ib$ is chosen from a Gaussian probability density function

$$p(a, b) = \frac{1}{2\pi} e^{-\frac{1}{2}(a^2+b^2)} \tag{2.8}$$

2.3 Adaptive Optics

We have introduced the concept of scattering media and we know light rays are strongly distorted by these media which greatly affects the image quality. It is necessary to correct these aberrations in order to achieve a high resolution image.

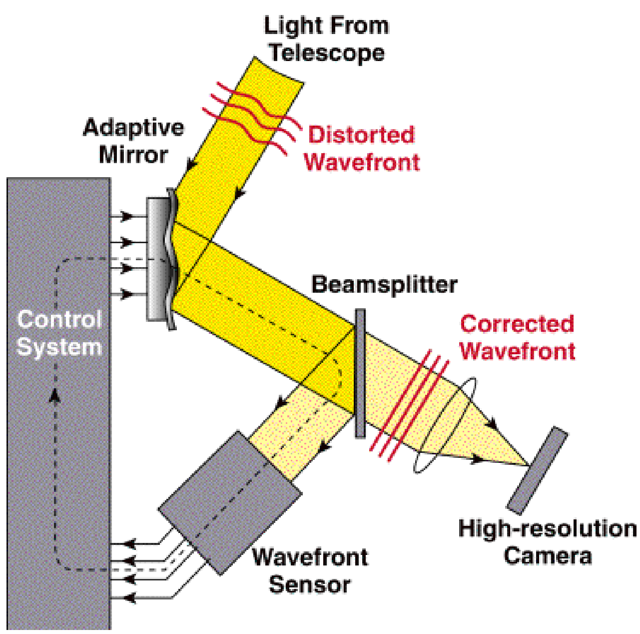

Figure 2.4: Scheme of an Adaptive Optics system [16].

Adaptive Optics (AO) has been widely used in astronomy for many years to correct the turbulence due to the earth's atmosphere [17]. An AO system usually consists of a wavefront sensing device, a wavefront corrector and a feedback imaging system, as shown in Figure 2.4.

The incoming light from a star is sensed by a wavefront sensor and then corrected by a wavefront corrector such as a deformable mirror (DM). Finally, the conjugated wavefront is focused on a high-resolution camera to create an image. Figure 2-5 displays a comparison of Near-infrared images of Uranus without and with adaptive optics.

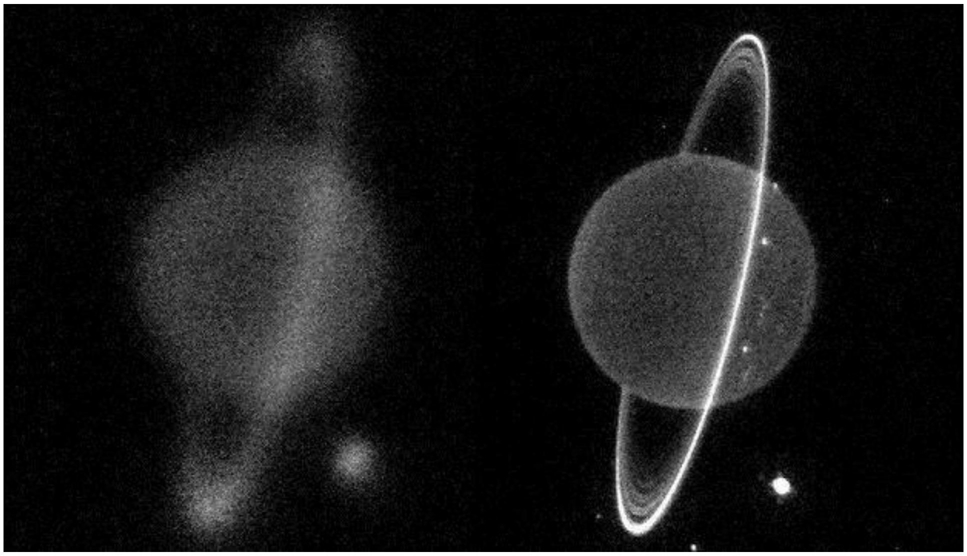

Figure 2.5: Near-infrared images of Uranus without(left) and with adaptive optics(right) [18].

The conventional adaptive optics system needs a wavefront sensor to measure the aberrations directly. The most commonly used wavefront sensor is the Shack-Hartmann Wavefront Sensor (SHWFS). It uses an array of lenses of the same focal length to create an array of image. The local tilt of the wavefront across each lens can be calculated from the position of the spot on the CCD or the photon detector [19]. But, another technique using a photodetector or a CCD camera instead of a wavefront sensor can be applied to determine the image quality. This wavefront sensorless adaptive optics system has been applied to the biological imaging field such as fluorescence and reflection microscopy [20, 21], two-photon fluorescence microscopy [22, 23] and optical tweezers [24, 25]. A similar wavefront sensorless method can also be used to correct the aberration caused by the scattering sample in our study. In scattering media, the anisoplanatic patch is essentially zero and many more segments are needed to correct aberrations for scattering media than for traditional AO.

The wavefront in conventional AO is typically described by Zernike modes, Equation 2.1. Its transmission matrix is structured with many zero elements and it has no more than a few hundred elements in contrast to the transmission matrix for a strongly scattering medium, Equation 2.9.

$$W_a = \begin{bmatrix} 0 & \dots & 1 & 0 \\ 0 & 1 & \dots & 0 \\ 1 & 0 & \dots & 0 \\ 0 & 0 & \dots & 1 \end{bmatrix} W_b \tag{2.9}$$

Where W_a is the wavefront after and W_b is the wavefront before. The wavefront is described by a column vector of the coefficients of the Zernike modes.

$$W = \begin{bmatrix} a_0 \\ \vdots \\ a_n \end{bmatrix} \tag{2.10}$$

Where the wavefront in the back pupil plane is

$$W(x,y) = \sum a_i Z_i(x,y) \tag{2.11}$$

2.4 Phase Conjugation

The aberrated wavefront can be corrected using phase conjugation both with a Deformable Mirror and with a Spatial Light Modulator. Phase Conjugation is accomplished by delaying the wavefront where it is ahead to let the rest of the wavefront catch up with it [26]. The shape of a DM is adjusted to conjugate the aberration. Figure 2.6 shows wavefront correcting using a DM. Before correction, the wavefront goes ahead a distance d than others. If the DM changes to a concave shape with a deep of $d/2$, then the wavefront reflected from the DM is the same.

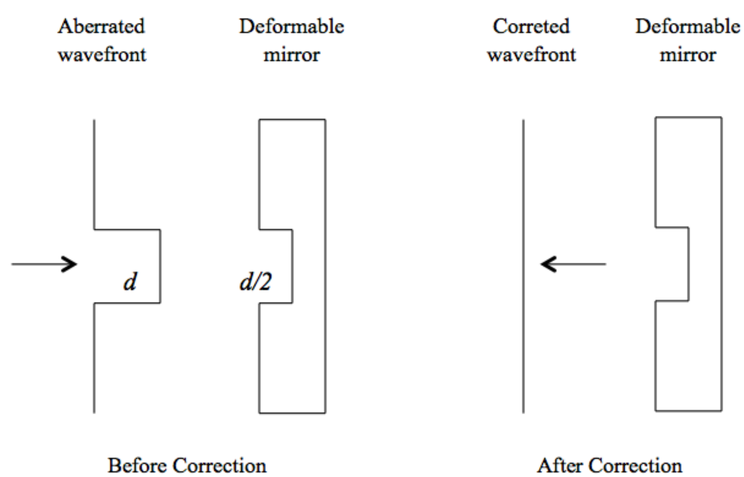

Figrue 2.6: Wavefront correction with a DM.

And for a SLM, it can change the index of refraction by tilting the liquid crystals. Figure 2.7 displays a wavefront correction with a SLM. Before correction, the light has a phase error $\Delta\varphi$ and the electric field $E = Ae^{i\Delta\varphi}$. If we set a phase value φ_1 on SLM, the new electric field $E' = Ae^{i(\Delta\varphi+\varphi_1)}$. φ_1 is the phase of the complex conjugate. We change the index of refraction on SLM and find a phase value $\varphi_1 = -\Delta\varphi$, then $E' = E$. Finally, the wavefront reflected from the SLM is the same.

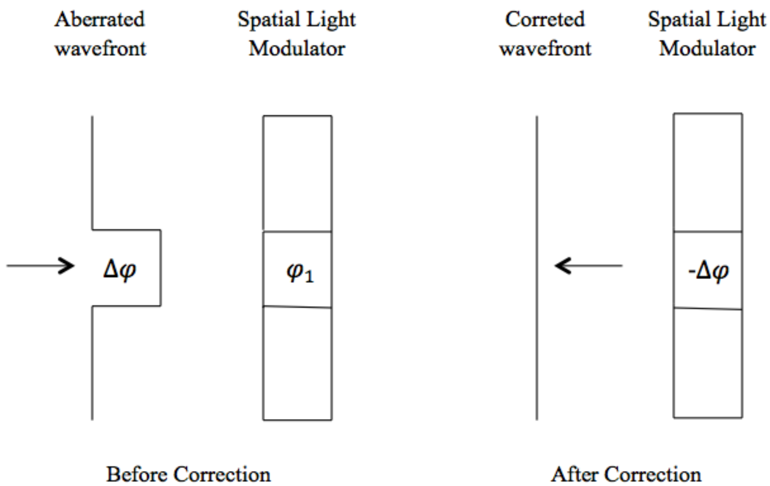

Figure 2.7: Wavefront correction with a DM.

CHAPTER 3

EXPERIMENTAL METHODS

3.1 Introduction

In the previous chapters we have looked at the concepts of the wavefront and adaptive optics. A conventional adaptive optics system should have a component to sense the wavefront with high spatial resolution and give feedback to the system [27]. Also, it must have the key element, a wavefront modulator or corrector to receive the feedback and apply a high speed, real-time correction. Wavefront correctors work like the same mechanisms that cause distortion. An aberrated wavefront can be corrected or compensated by another distorted mirror with proper shape, and this adjustment should be controlled precisely in order for the aberrations to be corrected at the image plane.

Usually, wavefront correctors are classified into two main categories. The first type is called inertial elements [17]. These are normally optical surface mirrors which are mechanically deformed to change the optical path length of a reflected beam of light. The most commonly used are Deformable Mirrors (DM). The second type of wavefront corrector is based on refraction. These devices contain birefringent optical materials that can change the index of refraction in response to an input such as an applied voltage. The change in refractive index modifies the velocity of propagation, thus changing the optical path length just like the first type described above [17]. Among these components, liquid crystal phase modulators are mostly used, and they are usually electrically controlled. In our experiments, we employ a Liquid Crystal Spatial Light Modulator (LC-SLM) and a Digital Micromirror Device to modulate the wavefront. In contrast to the conventional deformable mirror, these devices have many more pixels and the phase change can be discontinuous from pixel to pixel. These devices are described below.

3.2 Liquid Crystal Spatial Light Modulator

Liquid crystals were first examined by an Austrian botanical physiologist, Friedrich Reinitzer, in 1888. They are an intermediate state of matter between conventional liquids and crystalline solids, which retain the ordered characteristics of the crystalline, while having the flow properties of a liquid [17]. Liquid crystals have three main categories: Nematic, Smectic and Cholesteric. The most important property of liquid crystals is that the molecular orientation is changed in an electric field. Because the molecules have an anisotropic dielectric tensor, the change in molecular orientation results in a change in the index of refraction at the same time. Because of this, liquid crystals can be used to modulate the optical path length electronically. There are liquid crystal quarter wave plates, half-wave plates, optical filters and spatial light modulators. Spatial Light Modulators (SLM) are pixilated device in which each pixel can independently modulate the optical path length. By changing of the index of refraction of the liquid crystal for the light traveling through, the phase of the light is changed based on Equation 3.1.

$$\varphi = \frac{2\pi n x}{\lambda} \tag{3.1}$$

where n is the index of refraction and λ is the wavelength of light.

And the electric field is defined by Equation 3.2.

$$E(x,t) = Ae^{\frac{2\pi j n x}{\lambda}} \tag{3.2}$$

where A is the amplitude.

A phase only SLM will modulate the phase of the reflected beam from each pixel. For an input field E_{in}, the output field will be

$$E_{out} = E_{in} e^{j\varphi(x,y)} \tag{3.3}$$

The electric field is perpendicular with the SLM cover glass. The liquid crystals are parallel with the SLM cover glass if there is no voltage on the pixel and the difference between the extraordinary index of refraction (n_e) and ordinary index of refraction (n_o) is the largest, Figure 3.1(a). The phase delay is the maximum under this state. If the voltage on the pixel increases, the liquid crystal starts to tilt until reaching its extreme status. In this case, the difference between n_e and n_o is close to zero and the phase delay is minimum, Figure 3.1(b).

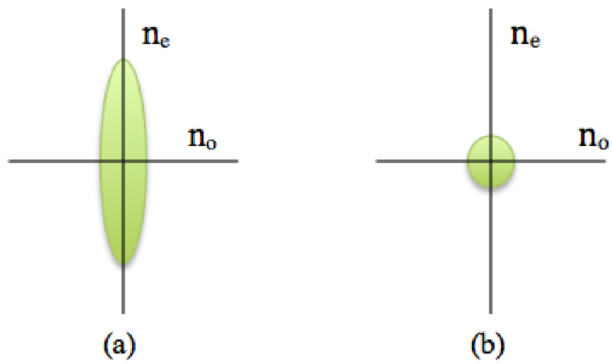

Figure 3.1: Status of liquid crystal under two voltage states. (a) No voltage is applied. (b) Voltage is applied.

There are two types of Liquid-Crystal SLMs based on different readout types: Transmissive SLM and Reflective SLM. The structures of optically addressed spatial light modulator are shown in Figure 3.2. The Transmissive SLM is a two dimensional membrane, and light is spatially modulated while passing through it according to the transmittance T(x(t),y(t)) at that certain point (x,y) and moment t. However, light is reflected from a reflective SLM with a phase modulation based on the reflectance R(x(t),y(t)).

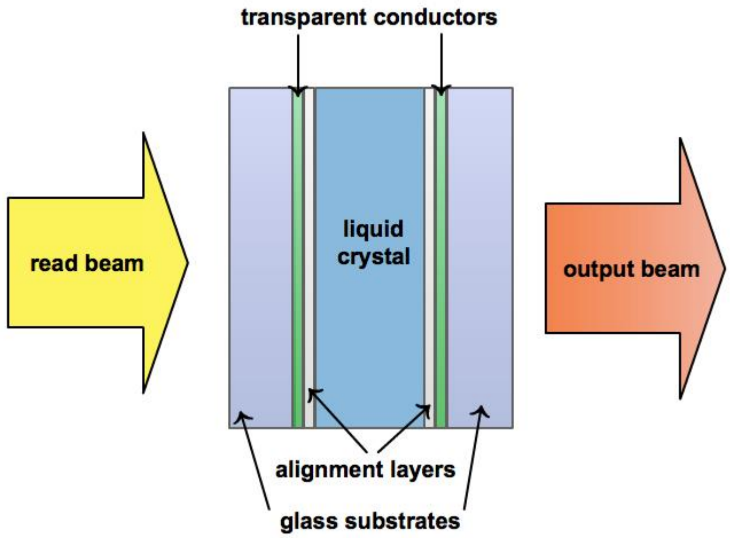

(a)

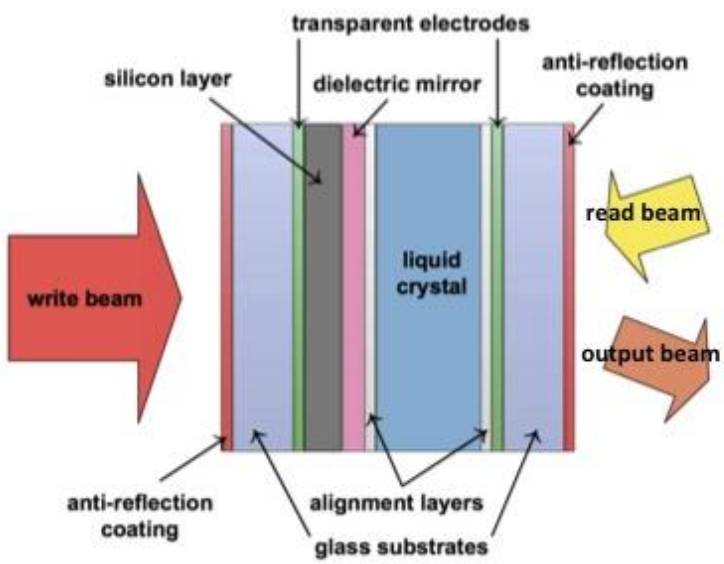

(b)

Figure 3.2: Structure of different SLMs. (a) Transmissive SLM, (b) Optically Addressed Reflective SLM [28].

A SLM can easily and rapidly change the wavefront of a coherent light beam with high speed by converting digitized data into optical information. The key element of a SLM is the central part which contains M×N liquid crystal pixels (512×512 in our case). M and N represent the number of pixels in Y rows and X columns, respectively. Each pixel also consists of several liquid molecules. Figure 3.3 below illustrates the basic structure of the pixel square. Pixels pitch is defined as the distance between the centers of two neighboring pixels. And the interpixel gap is the distance between the edges of two adjacent pixels.

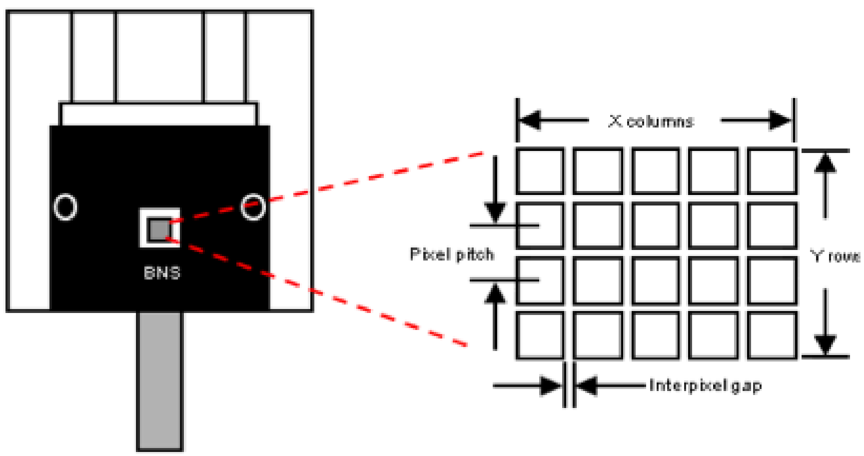

Figure 3.3: Pixel structure of SLM. They are arranged in an XY pattern [29].

An SLM is an electrically programmable device and it consists of a Cover Glass and a Transparent Electrode at the top; a VLSI Die, Pixel Electrode and a Pin Grid Array Package at the bottom; and a layer of birefringent Liquid Crystals between both of them. The collimated light enters SLM from the top, and passes through the liquid crystals, and then reflects back by the pixels at the bottom. The pixels are connected with the VLSI backplane through a circuitry, Figure 3.4.

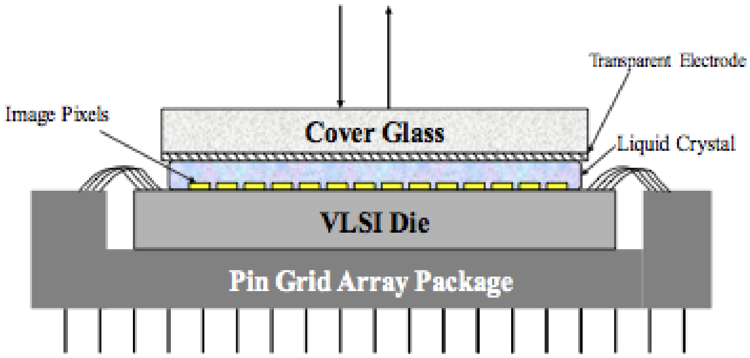

Figure 3.4: A cross section of SLM [29].

The pixels have discrete voltage states, but the phase response on SLM to the applied voltage is nonlinear. By using a custom look-up-table (LUT), the phase response is a linear value from 0 to 2π. Figure 3.5 displays the phase delay under 4 voltage states. The third one (5V) is apparently going faster than the first one (0V).

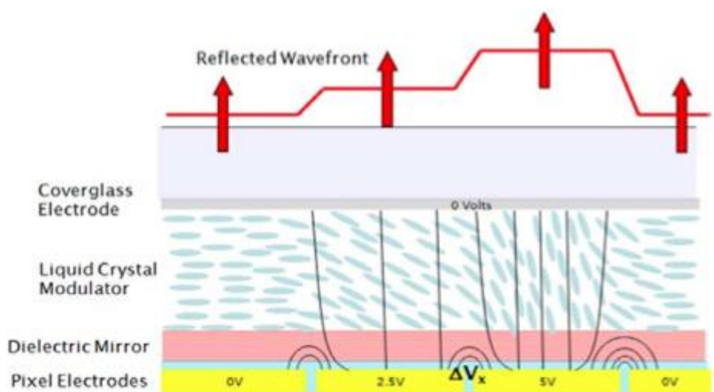

Figure 3.5: Phase delay under different voltages [29].

The Spatial Light Modulator in our experiment is a nematic liquid crystal XY Phase Series SLM fabricated by Boulder Nonlinear Systems, Inc.. The parameters referred to Table 3.1.

Table 3.1 Parameters of the boulder nonlinear systems nematic liquid crystal XY Phase Series SLM

Parameter	Array Size	Pixel Pitch	Switching Speed	Number of Discrete Voltages	Phase Range
Value	512×512	15×15 μm	100 HZ	65535	0~2π

Many research groups have developed several phase modulation algorithms based on SLMs, such as Sequential Algorithms [5] and Transmission Matrix methods [8]. And we will talk about these algorithms in details in Chapter 4.

3.3 Digital Micromirror Device

The Digital Light Processor is a type of projector technology that uses a digital micromirror device (DMD). Each mirror can tilt either +12° or -12° from the projector plane along the DMD diagonal, see Figure 3-6. If the light source is placed at -24°, the mirror is turned on by tilting it to-12°. This can be done by set a value of 255 (8-bit) on the pixel. And in the same way, the mirror is turned off by tilting it to +12° (pixel value is 0). A DMD can generate a binary amplitude pattern while a SLM generates a light beam with different phase values.

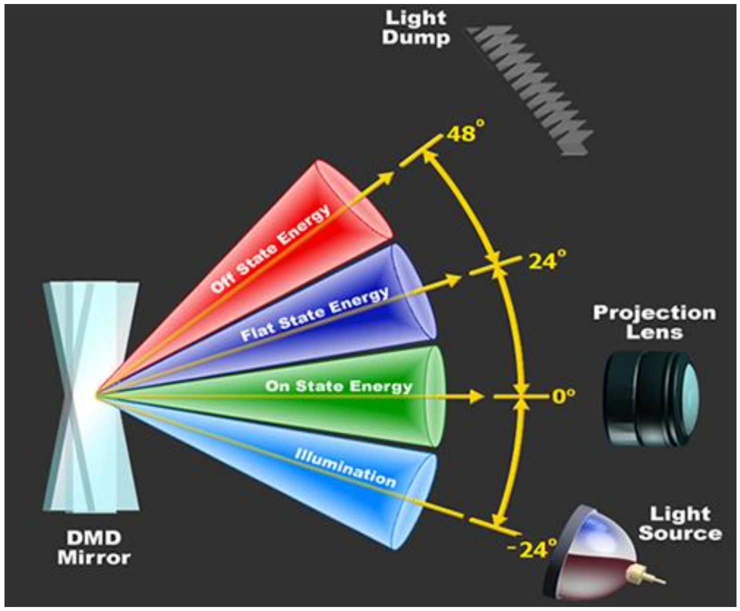

Figure 3.6: Diagram of a Digital Micromirror [30].

The pixel consists of a mirror attached by means of a via to a hidden yoke and a torsional hinge. The yoke makes contact with the surface below on the spring tips shown in Figure 2. The diagram also shows a mirror in each of the two stable states. The yellow electrodes shown are used in holding the mirror in these positions [31].

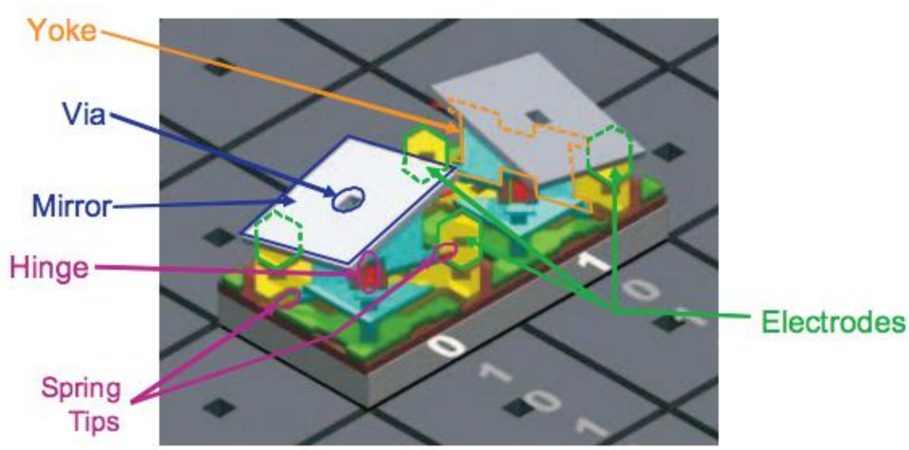

Figure 3.7: Pixel with labeled parts [31].

Below each mirror is a memory cell formed from Dual CMOS memory elements, Figure 3.8. The state of the two memory elements are not independent, but are always opposite. If one element is 1, the other element is 0 and vice versa [31]. In this way, the memory cell can control the two statuses of the DMD.

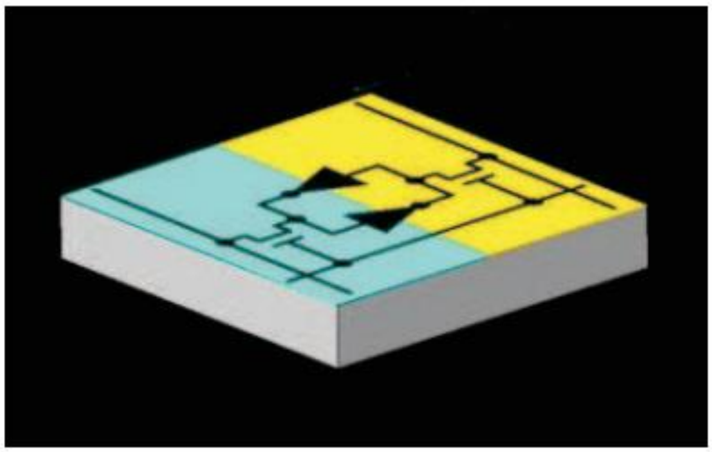

Figure 3.8: Dual CMOS pixel memory [31].

The DMD in our experiment is Texas Instruments 0.7" XGA DLP-D4000 development kit. The parameters refer to Table 3.2.

Table 3.2 Parameters of TI XGA DMD

Parameter	Array Size	Pixel Pitch	Switching Speed	Status
Value	1024×768	13.6×13.6 μm	32550 HZ	$0\ or\ 1$

3.4 Experimental Setup

Experiments were performed with both a Spatial Light Modulator (SLM) and a Digital Micromirror Device (DMD). Experiments with phase only modulation and binary amplitude modulation were both performed with a SLM.

The experimental setup for the DMD is shown in Figure 3.9. A polarized laser beam (1.5mW 543nm HeNe laser, Newport Corp.) is collimated and expanded, and then illuminates the DMD with a high switching rate of 32,550 patterns per second. While the DMD is capable of this high switching speed, the frame rate of the D4000 development kit is limited to ~1 kHz in practice.

By grouping sets of micromirrors together, the DMD is separated into a variable number of square segments, N. In the experiments, the DMD segments are turned off and on, using the algorithms described below, to reflect only light that is beneficial for maximizing the target intensity. Mirrors M3 and M4 are used to orient the incoming beam, so that the mirrors oriented in the +12° direction send the reflected beam toward the sample. The DMD is imaged onto the back aperture of the 10x objective at 1:1 with lenses Lc (f=120mm) and Ld (f=120mm) so that the short axis of the DMD fills the objective aperture. The light is focused through the scattering sample (A Ground Glass Diffuser, Thorlabs DG10-120-MD), and the second objective images the focal plane onto the CCD camera (Pike F-032B, 7.4µm pixel size, Allied Vision Technologies or CoolSNAP HQ2, 6.45 µm pixel size, PHOTOMETRICS) which provides the feedback for the binary modulation algorithms. For diffraction limited imaging, the diameter of the focused spot will be 4.8 pixels (λ/2NA) for the Pike F-032B camera.

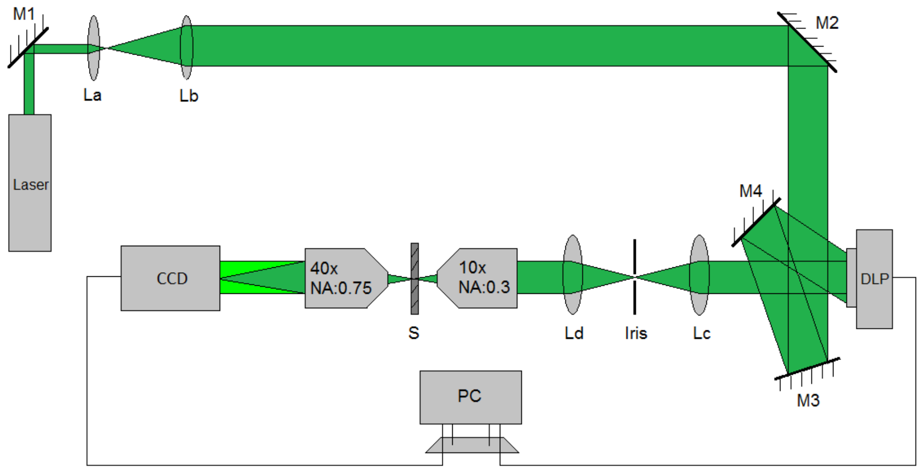

Figure 3.9: Schematic of the DMD experimental setup. A 543 nm laser beam is expanded and reflected off the DMD projector. The DMD is imaged by lens Lc and Ld onto the back aperture of the 10x objective and then focused onto the sample (S). A 40x objective is placed after the sample and the output intensity pattern is imaged by a CCD camera connected to the PC. ND: neutral density filter. Lenses: La, Lb, Lc and Ld. S: scattering sample. Mirror: M1, M2, M3 and M4. Distances shown in the figure do not represent the real experimental distances.

Experiments were also performed with a spatial light modulator (SLM) providing the binary amplitude modulation. The phase only SLM (512×512 high speed nematic SLM, Bounder Nonlinear Systems) was used to create a phase mask using methods described in [4], and create a binary amplitude pattern using the simultaneous amplitude and phase modulation method described in [15]. A schematic of the SLM experimental setup is shown in Figure 3.10.

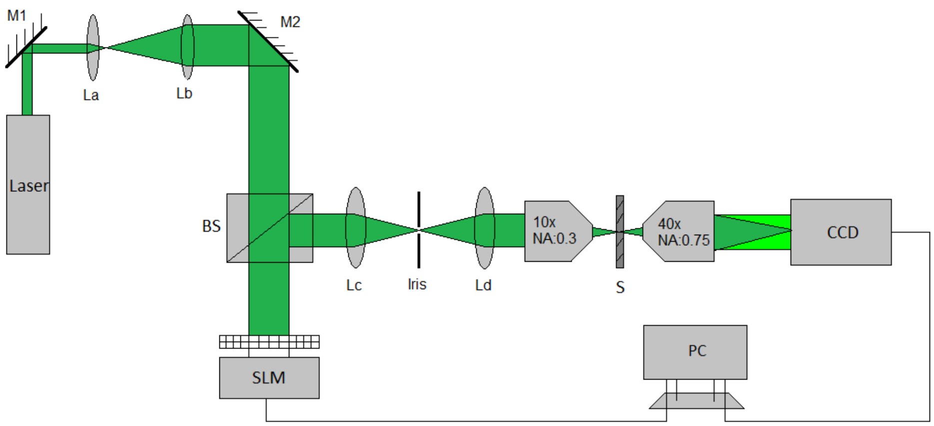

Figure 3.10: Schematic of the SLM experimental setup. A 543 nm laser beam is expanded and reflected off a liquid crystal spatial light modulator (SLM). The SLM is imaged onto the entrance pupil of the 10x objective at 1:1 by lenses Lc (f=120mm) and Ld (f=120mm). The Iris between the lenses is used to select the diffraction order which encodes the binary wavefront. The shaped wavefront is focused on the strongly scattering sample (S), and a CCD camera images the transmitted intensity pattern. M: mirror; BS: Beam Splitter. Distances shown in the figure do not represent the real experimental distances.

3.5 Scattering samples in our experiment

We performed wavefront optimization to focus light through a Ground Glass Diffuser and latex beads. Both of them are strong scattering media and widely used in the literature. The type of Ground Glass Diffuser we used is DG10-120-MD designed by Thorlabs. It is very stable and has long persistence time limited only by the mechanical stability of the setup.

To create a strongly scattering sample, we have also embedded latex beads in polyacrylamide. Each latex bead acts as a Mie scatterer and the scattering mean free path and the persistence time can be controlled by changing the concentration of beads in the matrix. Polyacrylamide is a polymer which will harden after it is cross-linked making a fixed sample.

Spherical particles will scatter light in a well-understood manner (Mie scattering) so that the scattering coefficient for these types of samples can be estimated.

The protocol for making the sample is as follows:

1. Create a 10% by weight solution of Sodium Sulfite (J. T. Baker 3922-01) in water (i.e. 10 milligrams in 100 microliters).

2. Create a 10% by weight solution of Ammonium Persulfate (Fisher BioReagents BP179-100) in water.

3. 450nm diameter latex beads in solution in DI water at a concentration of 4% weight/volume (Molecular Probes C37269) were used at the original concentration or diluted in DI water by a factor of 2 to make a 2% weight/volume ratio solution.

4. Mix 45µl of bead solution, 45µl of Polyacrylamide (30%) and 20 µl each of the solutions created in step 1 and step 2. Put in the solutions from 1 and 2 last because the polymer will immediately begin to harden after these are added.

5. Immediately put ~40 µl onto slide and cover with coverslip.

3.5.1 Scattering properties of Latex bead samples

We can estimate the scattering length for this sample from Mie theory. The parameters of latex bead are shown in Table 3.3.

Table 3.3 Parameters of Latex Beads

Parameter	Diameter	Density	Index of refraction	Concentration
Value	D = 450 nm	ρ =1.055 g/ml	n = 1.591	$c = 2\% \ w/v$

The mass of particles in 1 ml is $M = cV\rho = 0.02g$. And the volume of a particle is $V = \frac{4\pi}{3}(\frac{D}{2})^3 = 0.0477\ \mu m^3$. The mass of a particle is $m = \rho V = 0.05 * 10^{-12}g$. The number of particles in 1 cubic micron is therefore $N = \frac{M}{m} = 0.39$. The scattering coefficient is $\mu_s = 235.29mm^{-1}$ calculated from [32]. The thickness of the sample is d = 0.17 mm. Therefore $e^{-\mu_s d} = e^{-39.95} \approx 0$. So after scattering, almost none of the rays remain the initial direction.

CHAPTER 4

WAVEFRONT OPTIMIZATION ALGORITHMS

4.1 Introduction

In chapter 3, we discussed how wavefront modulators work. In this section we will talk about how we control these wavefront modulators and what algorithms we use to correct and optimize the wavefront in order to create a clear focal spot on the target.

In this chapter, we discuss two basic wavefront correction methods: phase-only modulation and binary amplitude modulation will be introduced. For the phase-only modulation method, several algorithms including the Stepwise Sequential Algorithm, the Continuous Sequential algorithm, the Partitioning Algorithm, and the Transmission Matrix Algorithm are discussed. These methods have been introduced in [5, 6, 8]. For binary amplitude modulation method, we introduce the Genetic Algorithm and the Binary Transmission Matrix Algorithms.

4.2 Phase modulation Algorithms

4.2.1 Stepwise Sequential method [4, 5]

The SLM surface is divided into N square segments of equal size (each made up of one or more pixels), and a beam reflected from a certain segment contributes to the intensity on each target camera pixel individually. Thus, the stepwise sequential algorithm tries to manipulate each of the segments individually and find the optimal wavefront to concentrate all the light on one camera pixel. Figure 4-1(a) illustrates how this method works. Iteratively, the phase retardation φ on each of N segments is set to values between 0 and 2π (for instance, $\varphi = 0, \pi/2, \pi, 3\pi/2$), while setting all the remaining N-1 segments to a constant value of zero phase retardation as the background field. For one segment, the phase value that maximizes the target pixel intensity on the detector is stored and then the phase retardation on this segment is reset to zero again to keep the same background field. Then these steps are sequentially repeated for the next segment until all the segments have been measured. Finally, all the stored phases are set on the segments and an optimal phase pattern on the SLM is constructed to focus light through the scattering media onto the target pixel. The measurement time of this algorithm is determined by the switching rate of the Spatial Light Modulator, the number of segments N, and the number of phase values tested.

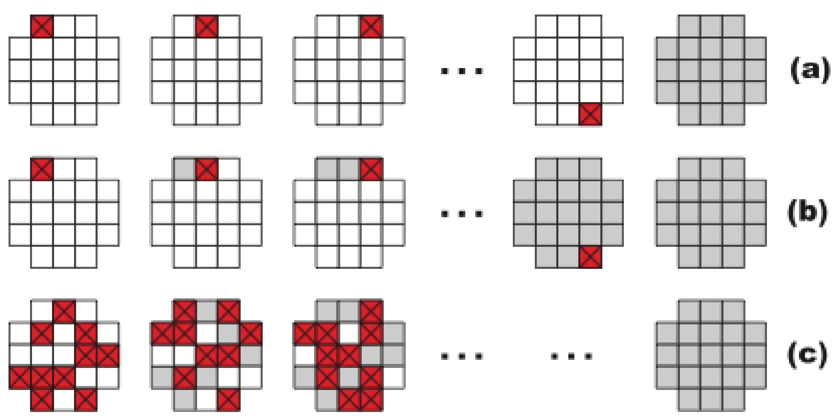

Figure 4.1: Principles of three sequential algorithms on SLM [4, 5].

4.2.2 Continuous Sequential method [5]

In most cases, the continuous sequential algorithm works similarly to the previous stepwise sequential algorithm. Figure 4-1(b) shows a few steps of this method. The phase retardation on each segment is iteratively set and the phase wich yields the maximum intensity is stored just like the stepwise sequential method. The only difference is that the phase retardation is not reset to zero again but updated to the new measured maximum value immediately after a measurement on one segment. In this case, the target pixel intensity and signal-to-noise ratio (SNR) begin to increase dynamically during the measurement.

4.2.3 Partitioning Algorithm [5]

The partitioning algorithm is different from the two former algorithms which manipulate each segment individually. In this approach, half of the segments are randomly chosen for each iteration and the same phase retardation between 0 and 2π is set on all the chosen segments simultaneously. Then, the computer determines the maximum value based on the CCD feedback and updates it immediately after each measurement. It is illustrated in Figure 4-1(c). After several iterations each segment will have a different phase because of the random partitioning.

4.2.4 Transmission Matrix method [8]

Besides the sequential algorithms above, there is another method in which the Transmission Matrix (TM) is measured directly to control the light [8]. The transmission matrix of an optical system is defined as a M×N matrix T of the complex coefficients t_{mn}, where M is the number of output modes, the pixels on the CCD, and N is the number of input modes, the pixels on the SLM. Then the transmitted outgoing electric field E_m^{out} of the *m*th mode is given by Equation,

$$E_m^{out} = \sum_n t_{mn} A_n^{in} \tag{4.1}$$

where A_n^{in} is complex amplitude of the incident light reflected from the *n*th input segment.

Now, we know the output electric field from Equation 4.1 then the intensity in the *m*th output mode for a given input phase retardation φ is given by Equation,

$$I_m^{\varphi} = |E_m^{out}|^2 = |\sum_n t_{mn} A_n^{in} e^{i\varphi}|^2 \tag{4.2}$$

In order to obtain the transmission matrix, a full field four phase method [10] is introduced. For each input mode, n, the computer iteratively sets the phase retardation to 0, $\pi/2$, π, and $3\pi/2$, and then measures the intensities in the *m*th output mode: I_m^0, $I_m^{\pi/2}$, I_m^{π} and $I_m^{3\pi/2}$, respectively. The measured transmission matrix element T is then,

$$T = \frac{I_m^0 - I_m^{\pi}}{4} + i\,\frac{I_m^{\frac{3\pi}{2}} - I_m^{\frac{\pi}{2}}}{4} \tag{4.3}$$

up to a multiplicative factor which is the same for all elements of the matrix. And the input vector for a desired focal spot at mth output mode is calculated by,

$$E^{in} = \frac{T^T E^{target}}{|T^T E^{target}|} \tag{4.4}$$

where T^T is the conjugate transpose matrix of T, and E^{target} is the output target vector with a value of 1 in mth mode, and 0 on the remaining modes.

Finally, the phases that maximize the global target intensity are calculated by,

$$\varphi_m = -\arg\left(E^{in}\right) \tag{4.5}$$

Another transmission matrix algorithm is reported in [8]. Instead of using the four-phase method, Conkey et al. introduce a three-phase method to recover the complex field. Three input phases φ= 0, $\pi/2$ and π are set on each segment, and the *m*th output mode intensities: I_m^0, $I_m^{\pi/2}$ and I_m^{π} are measured. The measured transmission matrix t_{mn} is calculated by,

$$T = \frac{I_m^{\pi} - I_m^{\pi/2}}{4} + i\,\frac{I_m^0 - I_m^{\frac{\pi}{2}}}{4} \tag{4.6}$$

and the input vector for a given *m*th output mode is calculated by,

$$E^{in} = \frac{T^t E^{target}}{|T^t E^{target}|} \tag{4.7}$$

where $T^t$is the transpose matrix of T

In both methods, the Hadamard matrix is used as the input basis when the computer sets the phase on SLM. The Hadamard matrix has a uniform amplitude of either +1 or -1 which perfectly fits the use of the phase modulation method [8]. Below, we discuss measurements using the four phase method using a pixel basis rather than the Hadamard basis.

4.3 Binary amplitude modulation methods

Many research groups have demonstrated methods for phase only modulation using spatial light modulators (SLM), including sequential algorithms [5], parallel algorithms [6], and genetic algorithms [7]. Another method only turns on the light rays that send light to the focal point. This approach, binary amplitude modulation, was first reported in [9].

In binary amplitude modulation, each segment, or channel, through the turbid medium is either on or off. This is in contrast to phase modulation in which the amplitude of each segment is the same but the phase is varied. In phase modulation, all the segments contribute to focus through the scattering medium. A comparison of the two different approaches is shown in Figure 4.2.

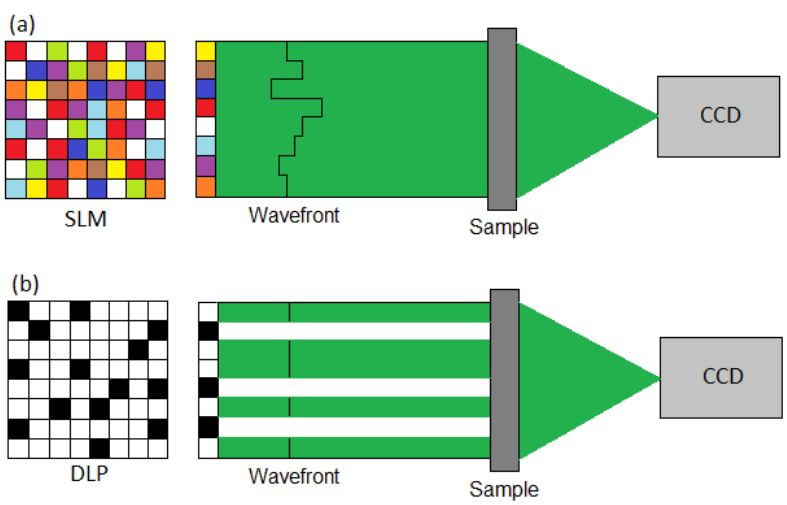

Figure 4.2: Comparison of phase wavefront optimization and binary amplitude wavefront optimization. (a) The phase of the wavefront is modulated. (b) The amplitude of the wavefront is modulated but the phase is not changed.

4.3.1 DMD based method

The binary amplitude modulation based on DMD is very straightforward. The micromirror on DMD has two statuses: 0 and 1. The binary mask can be easily generated by turning the mirrors on and off, which is described in detail in Chapter 3. Two binary algorithms based on the DMD were developed by Mosk [9] and Choi [33].

4.3.2 SLM based method

Since the SLM used in our experiment is a phase-only modulator, it cannot directly control the amplitude as the DMD does. Amplitude control can be achieved by combining multiple pixels. Combining two neighboring pixels was used in Birch's research [34]. Putten and Mosk [15] combined four neighboring pixels to control amplitude and phase with a phase-only SLM. This superpixel technique uses a phase difference of $\frac{\pi}{2}$ on each neighboring pixel to construct a complex value,

$$f = g + ih \tag{4.8}$$

Where g is controlled by the first and third pixel. h is controlled by the second and fourth pixel.

The fields modulated by the first and third pixel are given below.

$$E_1 = E_{1r} + i\Delta \tag{4.9}$$

$$E_3 = E_{3r} + i\Delta \tag{4.10}$$

Where E_{1r} and E_{3r} are the real parts of the fields, and Δ is the imaginary part.

$$g = E_1 - E_3 = E_{1r} - E_{3r} = (cos\,\varphi_1 - cos\,\varphi_3) + i(sin\,\varphi_1 - \sin\varphi_3) \tag{4.11}$$

For creating a binary amplitude, g should be a nonzero real value. This requires the imaginary part of g equals to 0.

$$\begin{cases} cos\,\varphi_1 - cos\,\varphi_3 \neq 0 \\ sin\,\varphi_1 - sin\,\varphi_3 = 0 \end{cases} \tag{4.12}$$

Thus, $\varphi_3 = \pi - \varphi_1$, and $g = 2\,cos\,\varphi_1$.

And h is constructed by the same way. The fields modulated by the second and fourth pixel are given below.

$$E_2 = E_{2r} + i\epsilon \tag{4.13}$$

$$E_4 = E_{4r} + i\epsilon \tag{4.14}$$

Where E_{2r} and E_{4r} are the real parts of the fields, and Δ is the imagery parts.

$$h = E_2 - E_4 = E_{2r} - E_{4r} = (cos\,\varphi_2 - cos\,\varphi_4) + i(sin\,\varphi_2 - sin\,\varphi_4) \tag{4.15}$$

The requirement is similar to the former one,

$$\begin{cases} cos\,\varphi_2 - cos\,\varphi_4 \neq 0 \\ sin\,\varphi_2 - sin\,\varphi_4 = 0 \end{cases} \tag{4.16}$$

Thus, $\varphi_4 = \pi - \varphi_2$, and $g = 2\cos\varphi_2$.

$$f = g + ih = 2\cos\varphi_1 + i2\cos\varphi_2 \tag{4.17}$$

The intensity is $f^2 = g^2 + h^2$. It is defined by the requirements below,

$$I = \begin{cases} zero, if\ \varphi_1, \varphi_2, \varphi_3, \varphi_4 = \left[\frac{\pi}{2}, \frac{\pi}{2}, \frac{\pi}{2}, \frac{\pi}{2}\right] \\ nonzero, if\ \varphi_1, \varphi_2, \varphi_3, \varphi_4 = \left[0, \frac{\pi}{2}, \pi, \frac{\pi}{2}\right] \end{cases} \tag{4.18}$$

By applying the phase retardation $\varphi_1, \varphi_2, \varphi_3, \varphi_4 = \left[\frac{\pi}{2}, \frac{\pi}{2}, \frac{\pi}{2}, \frac{\pi}{2}\right]$ on four neighboring pixels the segment, is turned off. And by setting $\varphi_1, \varphi_2, \varphi_3, \varphi_4 = \left[0, \frac{\pi}{2}, \pi, \frac{\pi}{2}\right]$ the segment is turned on, the modulated signal is emitted at an angle such that the phase difference between neighboring pixels is $\pi/2$, Figure 4.3. This diffraction angle must be selected with an iris. Using the phase retardation mask shown in Figure 4.4 (a), light focused after a Fourier lens creates the binary amplitude mask shown in Figure 4.4(b).

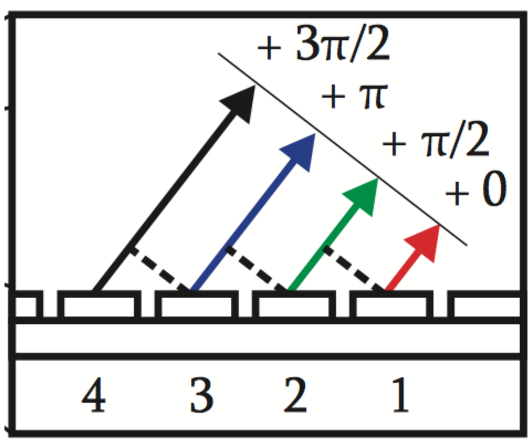

Figure 4.3: Theory of superpixel [18, 30].

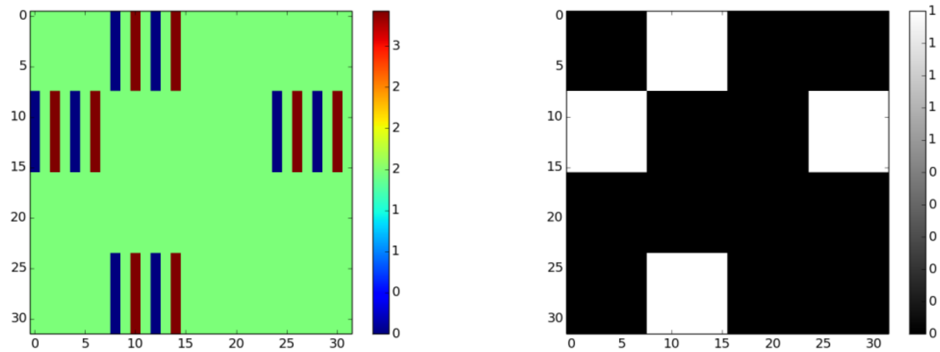

(a) (b)

Figure 4.4: Binary wavefront manipulation on SLM. (a) Phase retardation on SLM. (b) Corresponding binary amplitude mask of (a).

4.3.3 Genetic Algorithm

A general discussion of genetic algorithms (GA) can be found in [35]. Here we use an algorithm similar to that in [7]. Figure 4.5 shows the steps of GA method. First, an initial population of N parent masks is generated. Each mask contains a random binary value, 0 or 1 for each segment. The parent masks are iteratively written onto the DMD and the fitness of each mask is measured. The fitness in this method is defined as the intensity of a target pixel on the CCD output image. A ranking of the parent masks is conducted based on the fitness of each mask, according to the rule that higher intensity has a higher ranking. The next step is breeding: generating G new offspring from parent masks. Typically, we choose G=N/2. A parent mask with a higher ranking has a higher selection probability according to the following algorithm. To create the k^{th} child, the parents, ma and pa, are chosen from the N/2 highest ranked masks of the parent generation by comparing a uniformly generated number in the range 0 to $\sum_{\mathrm{n}=1}^{\mathrm{k}} \mathrm{n}$ to the value $\mathrm{p_j} = \sum_{\mathrm{n}=1}^{\mathrm{j}} \mathrm{n}$ for j=0 to k. This results in a higher probability of choosing parents with higher rankings.

Then a random binary template, T, is applied to generate an offspring mask that combines the parent masks, ma and pa, according to the Equation 4.19,

$$offspring = ma \cdot T + pa \cdot (1 - T) \tag{4.19}$$

After a new offspring is generated, a fraction, R, of elements are mutated. The mutation randomly switches the amplitude on a number of segments. The mutation rate R is defined by the Equation 4.20,

$$R = (R_0 - R_{end})e^{-\frac{n}{\lambda}} + R_{end} \tag{4.20}$$

where R_0 is the initial mutation rate, R_{end} is the final mutation rate, n is the generation number, and λ is the decay factor [7].

The new generation of offspring is then ranked by measuring the fitness of each member, and the members of the previous generation with lower ranking are replaced by these members of the new generation. Finally, a mask with a suitably high focal spot intensity is selected by iterating the above steps. The algorithm can be iterated a set number of times or stopped when the focal spot intensity reaches a specified threshold.

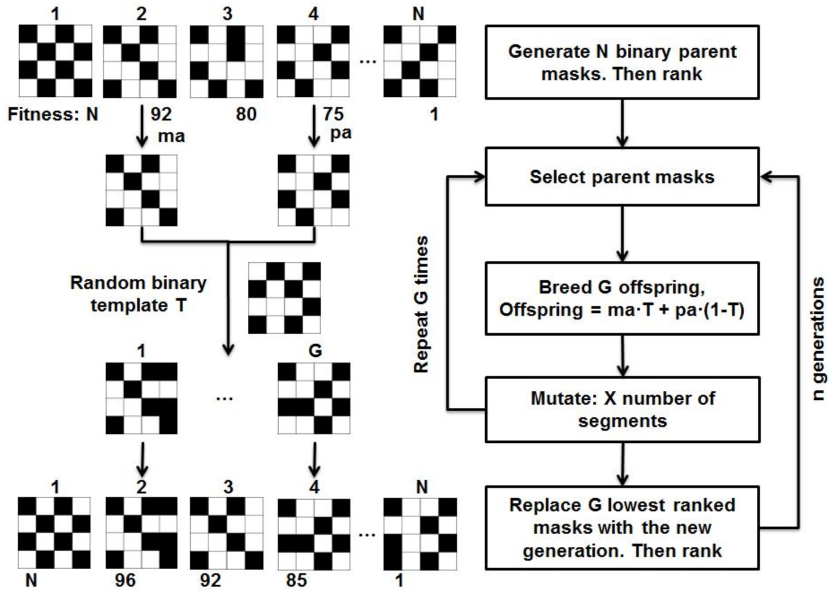

Figure 4.5: Steps in the genetic algorithm [7]. A population of binary masks is created and each individual is ranked according to the intensity at the desired focus. Parents are then selected with higher ranked individuals having a higher probability of being selected. The offspring is generated by combining the parent masks according to a binary template T. A fraction R of segments in the offspring is then mutated. After G offspring are generated, they replace the G lowest ranks members of the parent generation and the process is repeated.

4.3.4 Transmission Matrix Algorithm

In discussing the phase-only modulation methods, we have mentioned algorithms to calculate the transmission matrix [8]. In that case, we can only change phase value on one segment while keeping others as the same, but cannot manipulate a single channel while blocking light reflected from all the other channels. However, in binary wavefront correction methods, we can measure the output target intensity from a single channel without worrying about the interference from other channels since the mirrors or pixels can be turned on or off.

Because the transmission matrix is complex, it is generally necessary to measure or set both amplitude and phase. Choi [33] measured the transmission matrix for binary wavefront modulation, but he used an interferometric measurement at the CCD camera.

Here we introduce a method for calculating the transmission matrix up to an unimportant unitary matrix without measuring or setting the phase. For the *m*th output mode, we iteratively turn on each segment while turning off the others and measure the output intensities: $I_m^1, I_m^2,\ \ldots,$ $I_m^n, \ldots,\ I_m^N$, corresponding to each segment. This step takes N iterations. And the intensity form a single input mode, n, is given by Equation,

$$I_m^n = \left|t_{mn} A_n e^{i\varphi_m^n}\right|^2 \tag{4.21}$$

where A_n is the input amplitude of the nth mode. n is from 1 to N. φ_m^n is the phase on the nth segment. For an input with a uniform intensity and phase, I_m^n measures the magnitude squared of matrix element t_{mn}.

Next, we measure the intensity from the interference of two segments. For each iteration, we turn on the 1st and nth (n is from 2 to N) segments while turning off the other segments and the measured output intensities are $I_m^{12}, I_m^{13},\ \ldots,\ I_m^{1n}, \ldots,\ I_m^{1N}$, corresponding to each group of two segments. This step takes N-1 iterations. And the intensity is given by the Equation,

$$I_m^{1n} = \left|A_1 e^{i\varphi_m^1} + A_n e^{i\varphi_m^n}\right|^2$$

$$= \left|A_1 e^{i\varphi_m^1}\right|^2 + \left|A_n e^{i\varphi_m^n}\right|^2 + 2\left|A_1 e^{i\varphi_m^1}\right|\left|A_n e^{i\varphi_m^n}\right| \cos(\varphi_m^1 - \varphi_m^n)$$

$$= I_m^1 + I_m^n + 2\sqrt{I_m^1 I_m^n}\cos(\varphi_m^1 - \varphi_m^n) \tag{4.22}$$

Since we have already measured I_m^{1n}, I_m^1 and I_m^n, the phase difference is calculated by Equation,

$$\varphi_m^1 - \varphi_m^n = \cos^{-1}\left(\frac{I_m^{1n} - I_m^1 - I_m^n}{2\sqrt{I_m^1 I_m^n}}\right) \tag{4.23}$$

Assume φ_m^1=0, and we get φ_m^1, φ_m^2, … , φ_m^n, … , φ_m^N. Since the inverse cosine function generates both a positive and negative value, we will do one more step to determine the exact value of φ_m^n.

In the same way, we turn on the 2nd and nth (where n is from 3 to N) segments at the same time while turning off the others, and measure the new phase difference by Equation 4.22. This step takes N-2 iterations.

$$\cos\left(\varphi_m^{2'} - \varphi_m^{n'}\right) = \frac{I_m^{2'n'} - I_m^2 - I_m^2}{2\sqrt{I_m^2 I_m^2}} \tag{4.24}$$

where $\varphi_m^{n'}$ is the newly measured phase value. The phase value on the nth segment is determined by Equation,

$$\varphi_m^n = \begin{cases} \varphi_m^n, \left|\cos(\varphi_m^2 - \varphi_m^n) - \cos\left(\varphi_m^{2'} - \varphi_m^{n'}\right)\right| = 0 \\ -\varphi_m^n, \left|\cos(\varphi_m^2 - \varphi_m^n) - \cos\left(\varphi_m^{2'} - \varphi_m^{n'}\right)\right| = 2|\cos(\varphi_m^2 - \varphi_m^n)| \end{cases} \tag{4.25}$$

In practice, there will be noise in the measurements and neither equality will hold, so we use the following Equation to determine φ_m^n.

$$\varphi_m^n = \begin{cases} \varphi_m^n, \left|\cos(\varphi_m^2 - \varphi_m^n) - \cos\left(\varphi_m^{2'} - \varphi_m^{n'}\right)\right| \le \delta \\ -\varphi_m^n, \left|\cos(\varphi_m^2 - \varphi_m^n) - \cos\left(\varphi_m^{2'} - \varphi_m^{n'}\right)\right| > \delta \end{cases} \tag{4.26}$$

where δ is a small threshold value. It is set as 0.1 in our experiments.

Now, the phase φ_m^n of each matrix element is determined. The transmission matrix is determined up to a set of relative phase factors which do only affect the phase of the output which is not measured in any case, Equation 4.24.

$$\begin{bmatrix} \vdots \\ E_m \\ \vdots \end{bmatrix} = \begin{bmatrix} e^{-i\varphi_1} & & \\ & \ddots & \\ & & e^{-i\varphi_m} \end{bmatrix} T \begin{bmatrix} \vdots \\ E_{in} \\ \vdots \end{bmatrix} \tag{4.27}$$

The binary mask on the DMD or SLM is calculated by turning on the segment which only contributes to the focus spot at *m*th output mode. The binary mask $\mathrm{b_m}$ is given by the Equation,

$$\mathrm{b_n} = \begin{cases} 1, |\varphi_m^n| < \pi/2 \\ 0,\ \text{otherwise} \end{cases} \tag{4.28}$$

This algorithm has three steps and requires 3N-3 measurements. For example, if the number of segments N on the DMD is 16, 45 iterations are required. Figure 4.6 shows a 16×45 binary matrix. Each column is the status of the mirrors on DMD. White means that the mirrors are turned on inside the *n*th segment, while black means off.

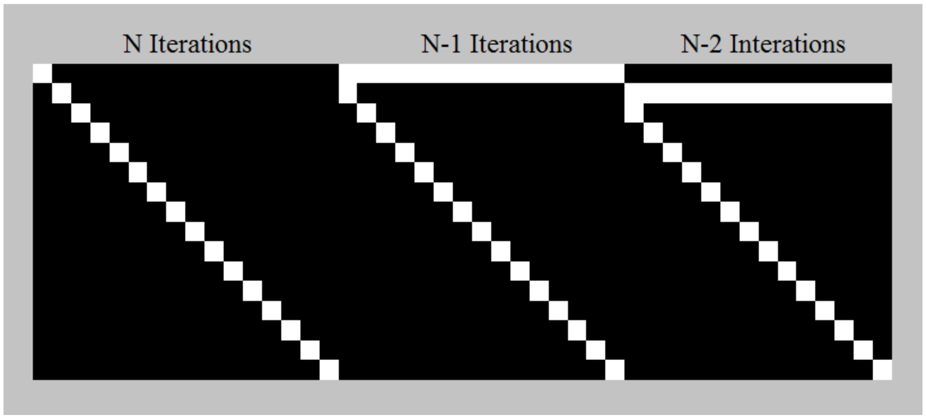

Figure 4.6: Illustration of the measurements for the binary transmission matrix measurement. The number of segments N is 16 in this case. Each column of the matrix represents the DMD settings for one measurement. White means on and black means off.

Finally, the desired binary mask b_n is constructed and written on the DMD or SLM, and a very clear and sharp spot will be seen on the CCD. Experimental results obtained with this algorithm will be presented in Chapter 5.

CHAPTER 5

RESULTS AND ANALYSIS

5.1 Introduction

In the previous chapters, the basic concepts for focusing in turbid media have been explained and two wavefront correction approaches, phase-only modulation and binary amplitude modulation, were introduced. Several algorithms based on these two concepts were also explained in detail. In this chapter, we present the results of our computer simulations and experimental measurements. The experimental results of focusing light through a ground glass diffuser and latex beads are presented and analyzed in detail. The results are compared with the simulations, and the advantages and weaknesses of the different methods are discussed.

5.2 Simulation of Phase-only Modulation

In chapter 2, we described the transmission matrix in the scattering media by the matrix t_{mn}.The electric field on the *m*th output mode is

$$\mathrm{E_m} = \sum_{n=1}^{N} \mathrm{t_{mn} A_n e^{i\varphi_n}} \tag{5.1}$$

where A_n is the amplitude of the incident light and φ_n is the phase retardation set on the nth segment of the SLM. Each element of the transmission matrix t_{mn} is chosen from a circular Gaussian probability distribution [4]. In this research, intensity enhancement is widely used as the measurement metric, and it is defined as the ratio of the maximal intensity after optimization to the average intensity before optimization. And according to [4], the enhancement is proportional to the number of segments N.

$$\eta = \frac{\pi}{4}(N - 1) + 1 \tag{5.2}$$

We simulate the turbid media using an M×N matrix of a Gaussian distribution, and take the angle of the sum of the complex values on each segment for the *m*th mode, $\varphi_n = -\arg T_{kn}$. Then we set the angles on each segment as the input field and the output field is the multiplication of the input field and the transmission matrix. Finally, a focus is achieved and its intensity is calculated by taking the square of the output matrix. The ideal simulation code is shown in the appendix A.1.

The simulated images before correction and after correction for the ideal simulation are showed in Figure 5.1. Figure 5.1(a) shows the image before correction. It is a completely random scattering image without any sharp focus spot and the intensities on each pixel are very low. Figure 5.1(b)-(e) illustrates the images after correction with a N=16, 64, 256, and 1024, respectively. From these four images, we can see that each of them has a focus spot at the center pixel even though the spot intensity is lower with lower N. However, the intensity in the focal spot becomes greater with an increasing number of segments N on the SLM. After a correction with N=1024 segments, the random background noise is dramatically suppressed relative to the focal spot, and an enhancement of 800 is achieved which is very close to the theoretical value.

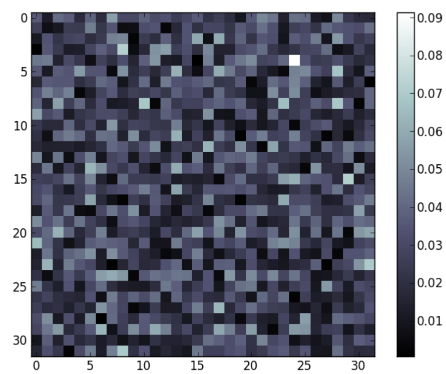

(a)

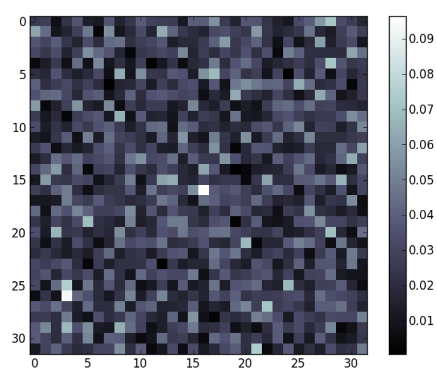

(b)

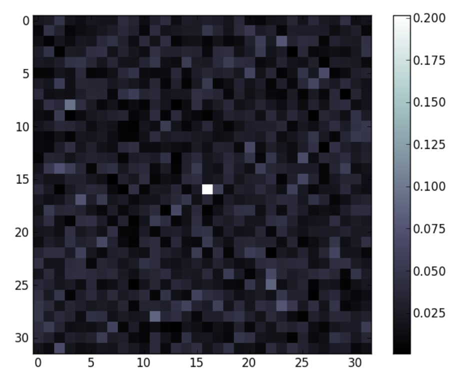

(c)

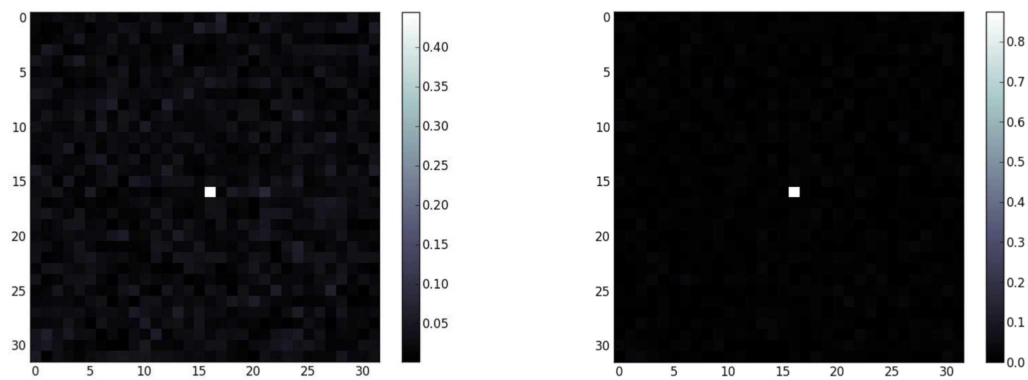

(d) (e)

Figure 5.1: (a) Simulated image before correction with random intensity. (b) Simulated image after correction with N=16 segments. (c) Simulated image after correction with N=64 segments. (d) Simulated image after correction with N=64 segments. (e) Simulated image after correction with N=1024 segments.

The sequential algorithm for phase modulation has been explained in Chapter 4. The enhancement plotted against the number of segments N for both the ideal simulation and the sequential algorithm simulation are shown in Figure 5.2. The blue curve represents the theoretical enhancement of Equation 5.2. The ideal simulation (green circles) is done by calculating the exact phase on each segment by choosing the phase value that maximize the target intensity. The enhancement calculated from the simulation of the sequential algorithm (red circles) is 25% lower. Both simulations are in agreement with the theoretical values and the enhancement is proportional to the number of segments used on the SLM.

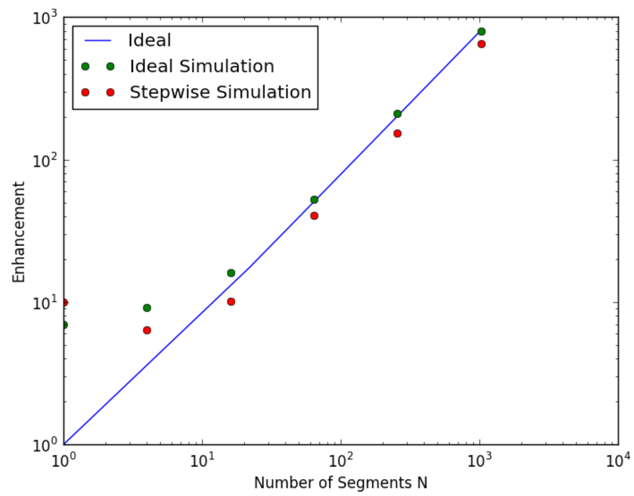

Figrue 5.2: A comparison of the two simulations with the theoretical value.

5.3 Experimental results of phase modulation method

From the simulations above, we know that the phase-only modulation method works very well for wavefront optimization. And experiments with different algorithms mentioned in Chapter 4 were conducted to focus light through a ground glass diffuser. Results are shown in Figure 5.3 and Figure 5.4.

During the measurements, the CCD exposure time was dynamically changed to maintain a good signal to noise ratio. After each iteration of the algorithm, the exposure time was automatically adjusted to maintain a maximum signal of 75% of the dynamic range. In calculating the enhancement, measured signals were scaled by the exposure time to be proportional to the intensity.

$$\eta = \frac{I_{after}/T_e}{I_{before}/T_e'} \tag{5.3}$$

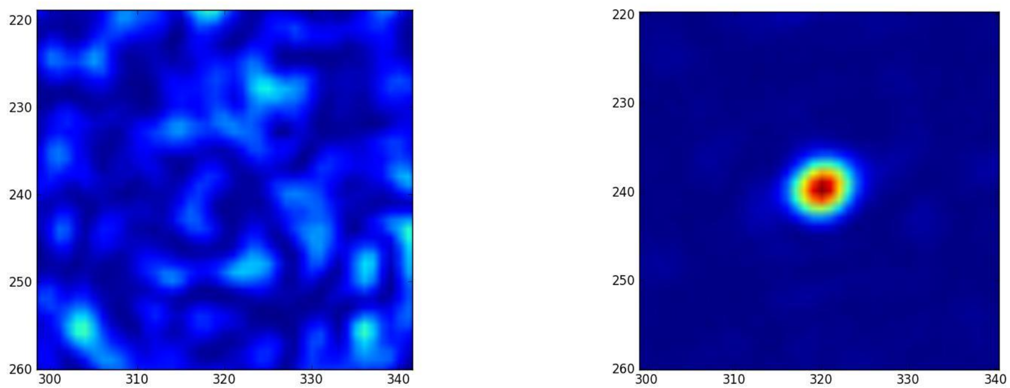

(a) (b)

Figure 5.3:. (a) Experimental image before correction. (b) Experimental image after correction with Stepwise Sequential Algorithm. Enhancement is 400 with N=1024.

Figure 5.3 displays the experimental images captured by a CCD camera before and after optimization with the sequential algorithm. The original image size is 768×1024. Here we show a region of interest (ROI) with a size of 41×41 in order to compare the images in detail. Figure 5.3(a) represents the image before correction. The image shows a random intensity pattern without any extreme sharp spots. However, Figure 5.3(b) shows the image corrected with the stepwise sequential algorithm. There is a clear and sharp spot in the image center with an enhancement of 400 using a number of segments N=1024 on the SLM.

In our experiments, both the Sequential Algorithm and Transmission Matrix Algorithm are tested with different parameters. For sequential algorithm, tests with both 4 phases ($\varphi = 0, \frac{\pi}{2}, \pi, \frac{3\pi}{2}$) and 8 phases ($\varphi = 0, \frac{\pi}{4}, \frac{\pi}{2}, \frac{3\pi}{4}, \pi, \frac{5\pi}{4}, \frac{3\pi}{2}, \frac{7\pi}{4}$) are performed. For transmission matrix algorithm, tests with 3 phases ($\varphi = 0, \frac{\pi}{2}, \pi$) and 4 phases ($\varphi = 0, \frac{\pi}{2}, \pi, \frac{3\pi}{2}$) are performed. Also, each test is conducted using different numbers of segments: N=4, 16, 64, 256, 1024, and 4096.

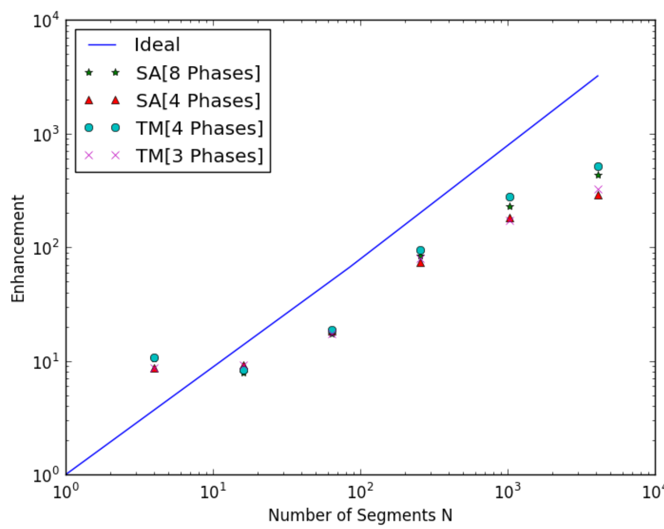

Figure 5.4: A comparison of Sequential Algorithm (SA) and Transmission Matrix (TM) Algorithm.

Figure 5.4 displays a comparison of the results with different algorithms. The enhancement is plotted against the number of segments N. The blue curve is still the theoretical value mentioned above (Equation 5.2). The green stars show the enhancement with 8 phases using the Stepwise Sequential Algorithm. The red triangles represent the enhancement with 4 phases with the Stepwise Sequential Algorithm. The results of the Transmission matrix algorithm with 4 phases are shown by the blue dots. And the red crosses illustrate the enhancement with the 3 phases Transmission Matrix Algorithm. All the algorithms demonstrate that the enhancement is proportional to the number of segments, N. But the enhancement is not close to the theoretical value of 3215 with N=4096. This test takes several hours and the error could be caused by vibration or drift of the optical system, or the persistence time of the scattering media. Nevertheless, all the curves show the same trend as the theoretical curve as expected even though the measured enhancement is not always as high as the value calculated with Equation 5.2. The phase-only modulation method works very well for focusing light through strong scattering media.

5.4 Experimental Results Affected by Persistence Time

In addition to experiments with a ground glass diffuser as the scattering sample, we have also used a sample of latex beads embedded in a polyacrylamide matrix as discussed in Section 3.5. While the ground glass diffuser has a very long persistence time limited only by the mechanical stability of the system, the stability of this sample can be controlled by the concentration of the latex beads in the polyacrylamide matrix. With a higher concentration of latex beads, the matrix does not solidify as effectively resulting in a shorter persistence time. The results of focusing through latex beads are displayed in Figure 5.5 and Figure 5.6.

Figure 5.5 displays the enhancement measured with short persistence time sample (4%w/v concentrations of latex beads). The sample was tested with N=4, 16, 64, 256, 1024, 4096. The green dots show the measured enhancement for different numbers of segments. For the first 5 values, the enhancement increases linearly with N, in general agreement with the theoretical value (blue curve). However, for the last test, the measurement has been conducting for more than 2 hours and it has already exceeded the persistence time of the sample. So the enhancement for final point N=4096 does not increase as expected.

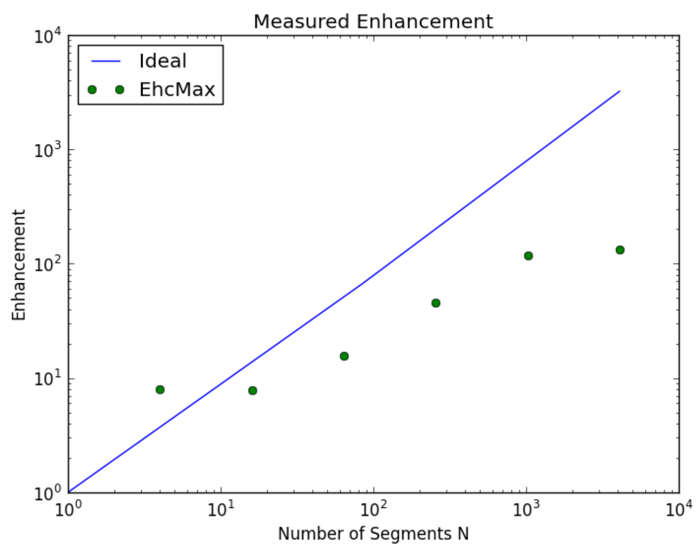

Figure 5.5: Enhancement of focusing through latex beads with short persistance time.

Since we know the persistence time affects light focusing, we made another sample with half the concentration of latex beads to remove the nomadic molecules which reduce the sample's stability. Figure 5.6 shows the results of focusing through a sample (2%w/v concentrations of latex beads) with a long persistence time. And after more than two hours' test, the achieved enhancements with four different algorithms are all in agreement with the theoretical curve. Many scattering samples have short persistence times. So, it is necessary to find an algorithm that works well and fast.

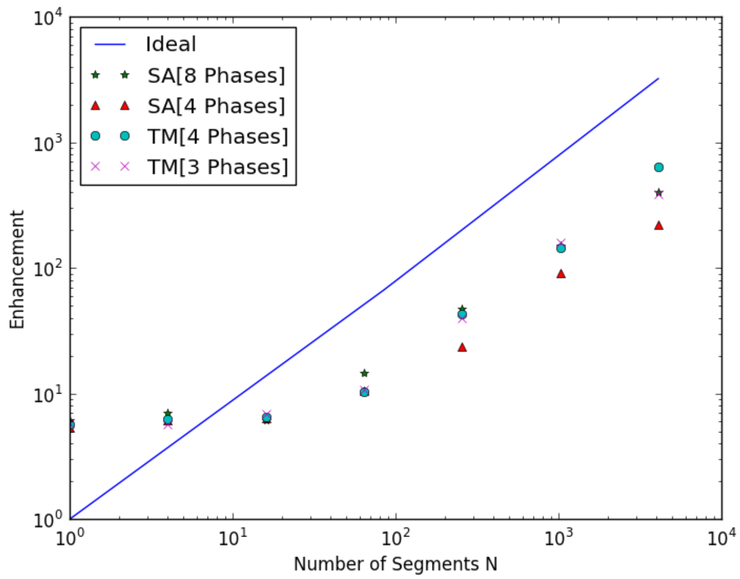

Figure 5.6: A comparison of enhancement for focusing through the long persistance time sample with different algorithms.

5.5 Simulation of Binary Amplitude Modulation

In order to study the feasibility and performance of binary wavefront optimization, we performed simulations to compare binary wavefront optimization with phase optimization and to compare different algorithms for binary wavefront optimization. The random media is modeled by a 1024×1024 random complex matrix with Gaussian statistics. Wavefront optimization with N segments can then be modeled by grouping the matrix elements by 1024/N, and we assume a camera with 1024 pixels. Optimal phase optimization is modeled by setting the SLM phase for segment n,

$$\varphi_n = -\arg \sum_{j=\frac{Mn}{N}}^{\frac{M(n+1)}{N}-1} T_{kj} \tag{5.4}$$

Here N is the total number of segments, M=1024 is the total number of scattering channels modeled by the matrix and k is the CCD pixel at the center of focus. For optimal binary wavefront optimization, segments are turned on only if they will add in phase.

$$b_n = \begin{cases} 1, |\varphi_n| < \pi/2 \\ 0, \text{ otherwise} \end{cases} \tag{5.5}$$

where b_n is the state of segment n, and φ_n is defined as above.

An example of optimal binary wavefront optimization is shown in Figure 5.7. Figure 5.7(a) shows the image before correction, and Figure 5.7(b)-(d) show correction with N=64, 256, and 1024 segments, respectively. Before correction, the image shows a random intensity pattern and there is no spot at the target position. After correction, the image shows a clear spot and the enhancement increases with the increasing number of segments.

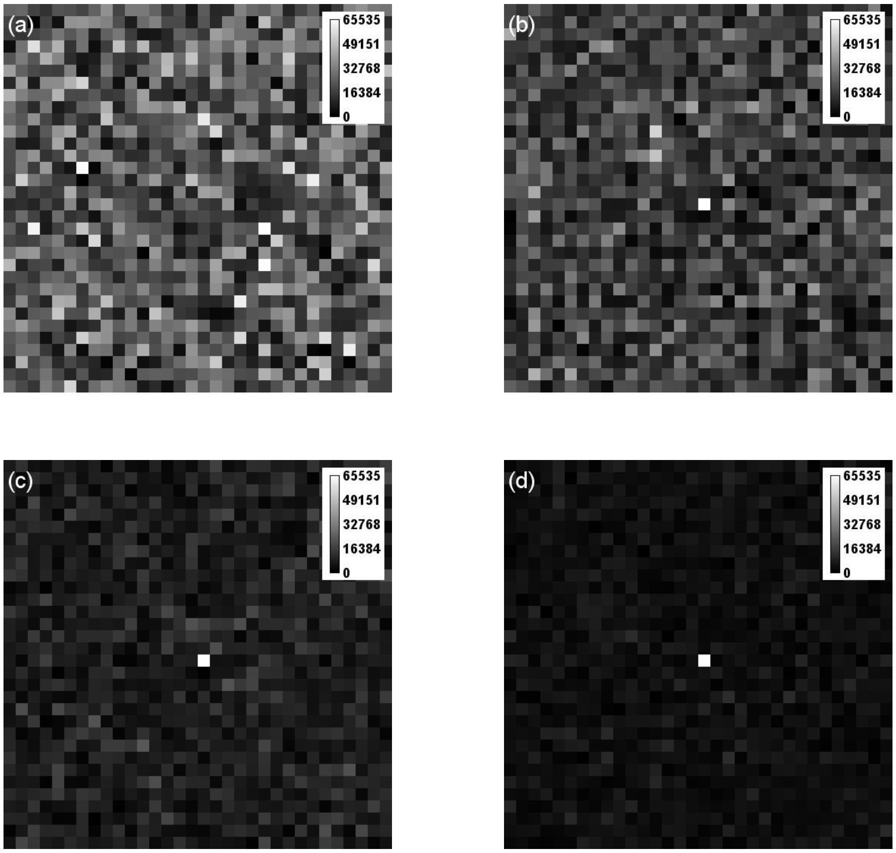

Figure 5.7: Results of simulations with optimal binary wavefront optimization. (a) Before correction. (b) Optimization with N=64. (c) Optimization with N=256. (d) Optimization with N=1024.

The enhancement plotted against the number of segments N is shown for both phase and binary wavefront optimization in Figure 5.8(a). The blue curve shows the theoretical enhancement for phase optimization, and the simulations of ideal phase optimization (green dots) and of the stepwise algorithm [5] (red crosses) are shown for comparison. The optimal binary wavefront optimization (blue triangles) results in an enhancement $\sim\frac{\pi^2}{2}$ smaller than what is possible for phase optimization, in agreement with the theory [9]. An enhancement comparison between ideal binary optimization (green triangles) and the genetic algorithm (red crosses) is shown in Figure 5.8(b). The blue curve shows the theoretical enhancement for binary wavefront optimization. The simulation shows that the genetic algorithm can achieve the maximum possible optimization of $\eta = \frac{N}{2\pi}$.

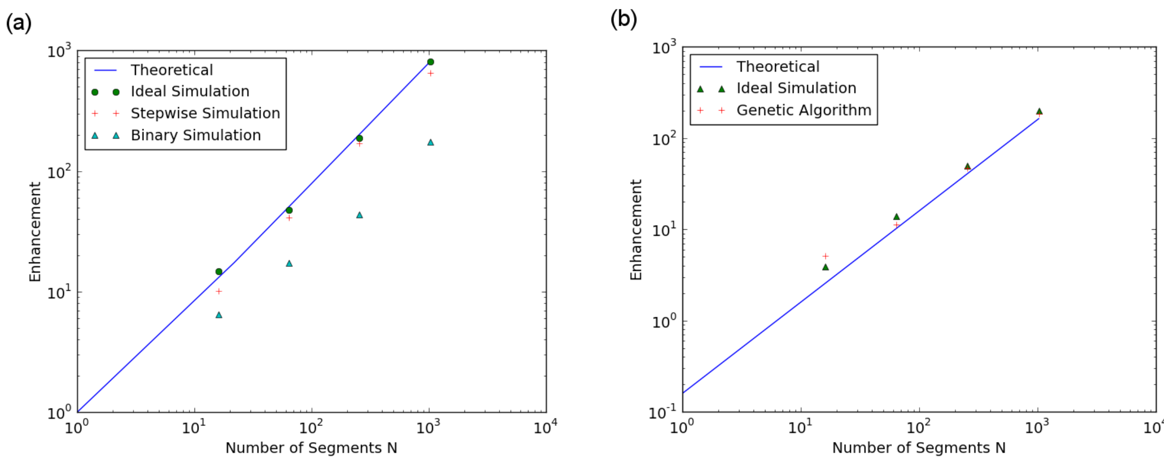

Figure 5.8: (a) Simulations of focusing through turbid media using phase and binary wavefront optimization as explained in the text. (b) Simulations of binary wavefront optimization.

5.5.1 Simulation of the Genetic Algorithm

A comparison of enhancement plotted against initial mutation rate is shown in Figure 5.9(a) for three simulations. The three approaches finally all go up to nearly the same enhancement. However, the simulation with initial mutation rate $R_0 = 0.01$ reaches the highest enhancement faster than those with $R_0 = 0.05$ and $R_0 = 0.1$. A comparison of enhancement plotted against population is shown in Figure 5.9(b). With a larger population, the algorithm needs a smaller number of generations to achieve the highest enhancement. However, each generation has to repeat more times to generate offspring, thus increasing the measurement time. So, the total measurement time is proportional to the population size, see Figure 5-9(d). Figure 5-9(c) shows a comparison of enhancement for different numbers of segments. The enhancement is, as expected, proportional to the number of segments. Appendix A.2 contains the code for Genetic Algorithm simulation.

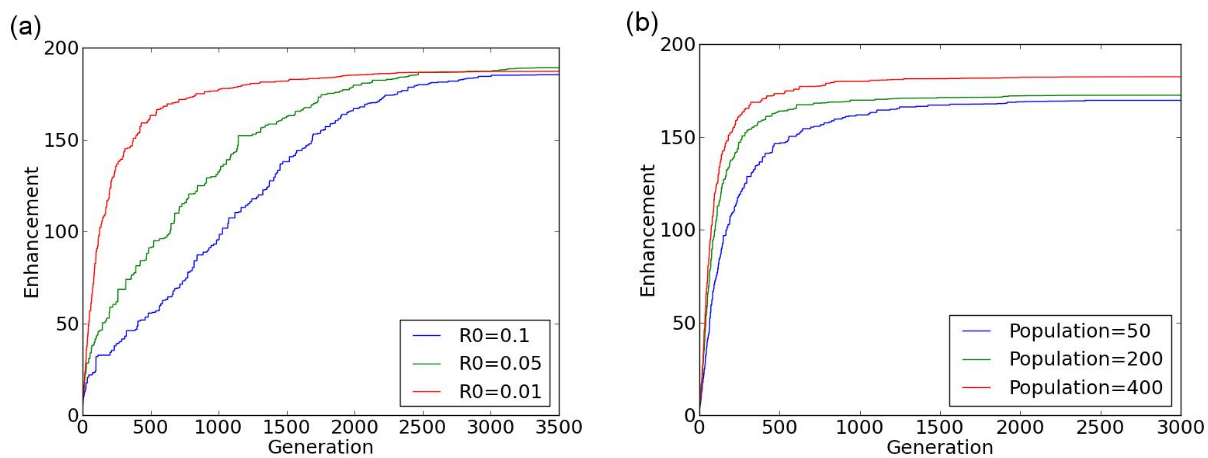

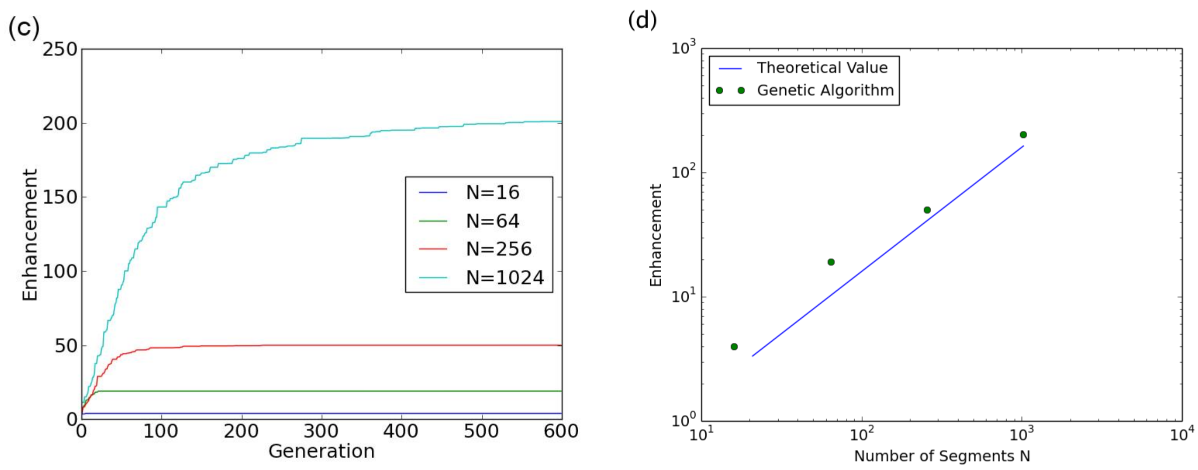

Figure 5.9: Simulations of binary amplitude modulation with the genetic algorithm for different parameters. (a) Comparison of different initial mutation rates with N=1024 segments and a population size of 50. (b) Comparison of different population sizes with N=1024 segments. (c) Comparison of different numbers of segments for a population size of 400. (d) Comparison of theoretical value and simulation value.

For the experiments described in section 5.6, the mutation rate is given by the following parameters: Initial mutation rate $R_0 = 0.01$; Decay factor $\lambda = 650$; Final mutation rate $R_{end} = 0.0025$.

5.6 Experimental Results of Genetic Algorithm

5.6.1. Experiments with a DMD

Figure 5.10 shows the results of optimizing the focus through the ground glass diffuser with the DMD. Before optimization, there is no focal spot at the target pixel, Figure 5.10(a). However, after 300 generations of the genetic algorithm on 3072 segments, there is a very clear spot at the target pixel with an enhancement of 117, Figure 5.10(b). The diameter of the focal spot is 8.9

pixels which is smaller than expected by diffraction. The scattering medium increases the effective numerical aperture [36]. The stepwise method did not produce a measurable enhancement. Figure 5.10(c) shows a horizontal profile through the focal spot after optimization. Figure 5.10(d) shows a Gaussian fit to the profile through the focused spot; the full width at half maximum is 5.24 pixels.

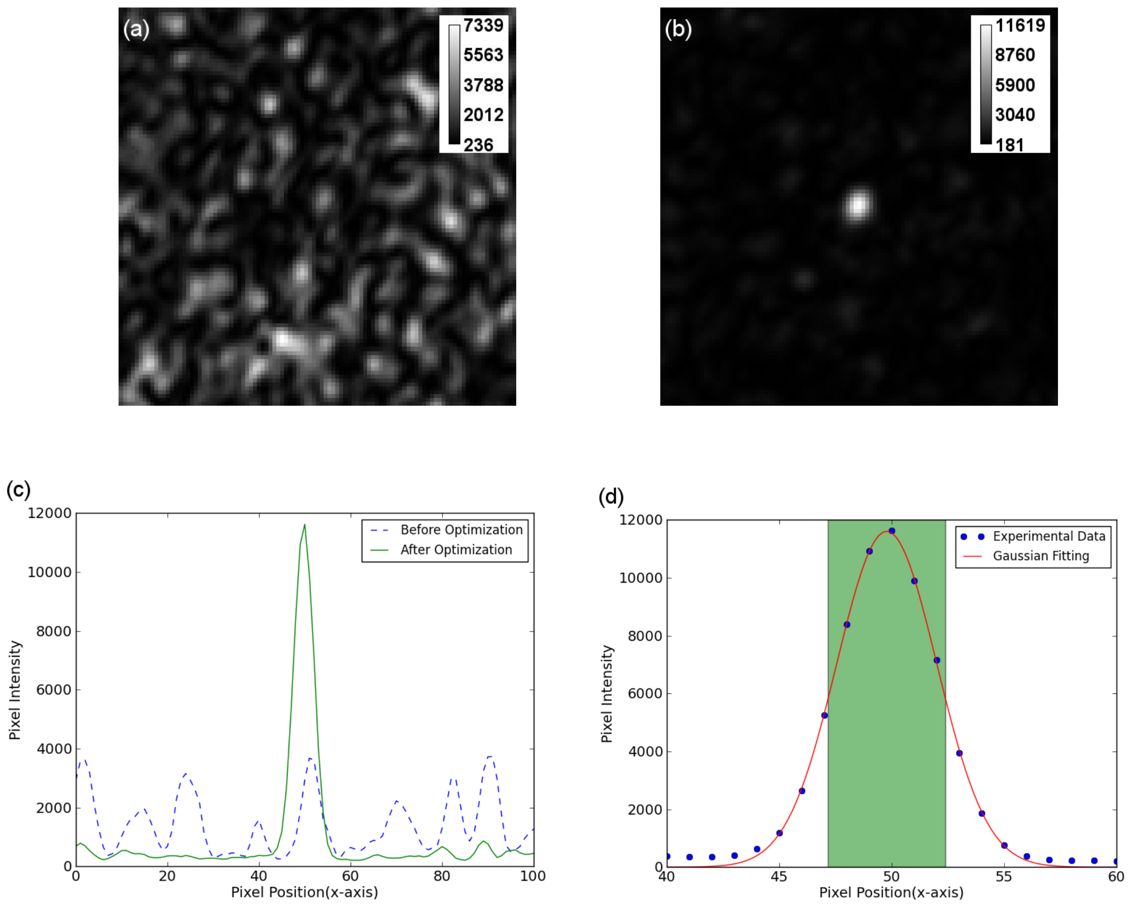

Figure 5.10: Focusing through a glass diffuser (a) Before correction. (b) After correction. For this experiment, the number of segments is 3072, the population for the genetic algorithm is 200, and the GA is run for 300 generations. (c) A horizontal profile through the focal spot. (d) A Gaussian curve fit to the horizontal profile. The green region signifies a range of pixels with intensity higher than half maximum.

Figure 5.11 shows the results of measurements on the DMD with different numbers of segments. Figure 5.11(a) shows a comparison of the enhancement between different numbers of segments. It indicates that the enhancement is proportional to the number of segments. Figure 5.11(b) show a comparison of the experimental results with theoretical values. The maximum enhancement is 117 after 300 generations with a population of 200 on 3072 segments.

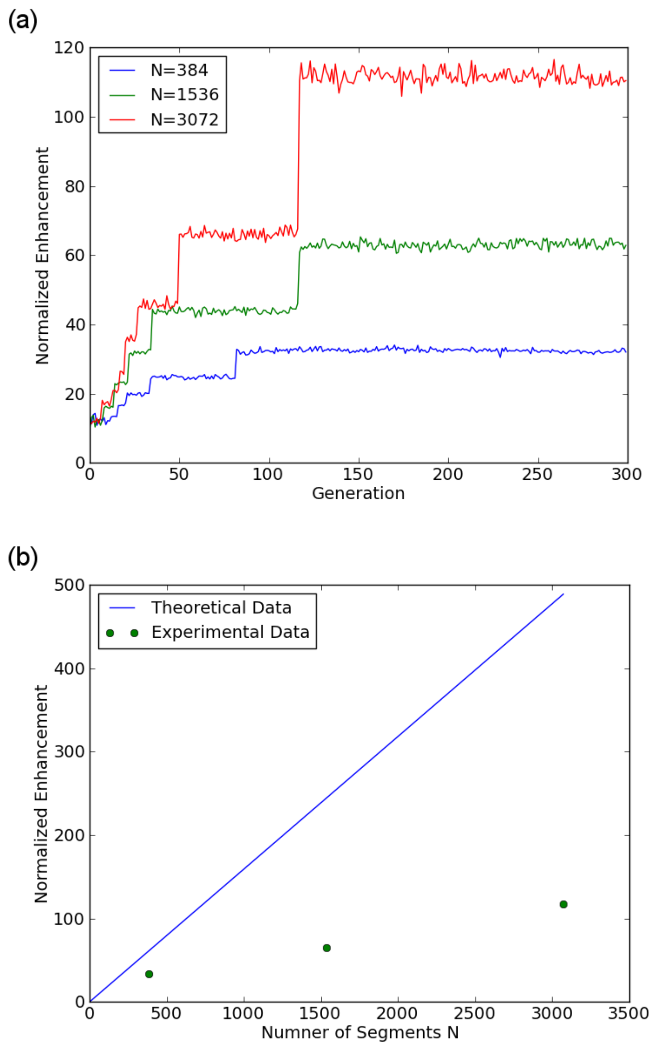

Figure 5.11: (a) Enhancement vs. generation for different numbers of segments. (b) Comparison of experimental results with the theoretical enhancement for phase modulation.

5.6.2. Experiments with the SLM

Figure 5.12 shows the results of focusing through the ground glass diffuser with the SLM. A comparison of enhancement plotted against generation number is shown in Figure 5.12(a). The maximum enhancement is 105 after 400 generations with a population of 200 on 1024 segments. The results agree with the theoretical simulation shown in Figure 5.12(b). Figure 5.12(b) show a comparison of the experimental results with the theoretical results ($\eta = \frac{N}{2\pi}$) for binary wavefront optimization.

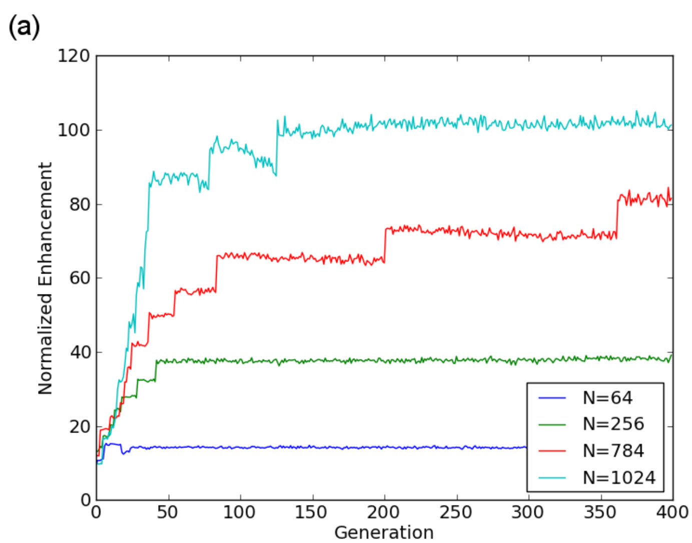

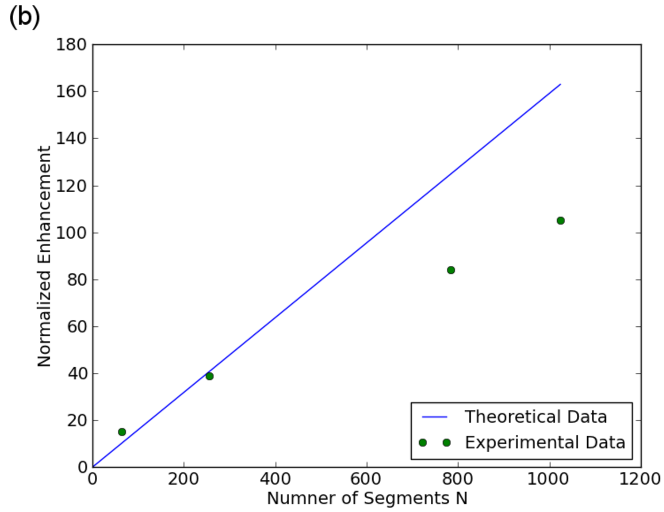

Figure 5.12: (a) Enhancement vs. Generation for different numbers of segments. (b) Comparison of experimental results with the theory for enhancement vs. number of segments.

5.7 Simulation of Transmission Matrix Algorithm

Before performing the Transmission Matrix algorithm on the DMD or SLM, simulations were also conducted to confirm the feasibility of the algorithm. Appendix A.3 contains the code for Genetic Algorithm simulation. Since this method manipulates a single channel at a time, the output intensity is very low. The low intensity makes this approach sensitive to the background noise. We simulate this situation by adding an offset to the output intensity. We simulate N=1024 segments.

Figures 5.13 to 5.15 show the results of the three steps of the Binary Transfer Matrix Algorithm on 1024 segments. Figure 5.13 (a) shows the output intensities on pixel m from the 3069 measurements (N measurements with a single segment, N-1 measurements with segment 1 and segments 2-N sequentially turned on, and N-2 measurements with segment 2 and segments 3-N sequentially turned on) required to determine the phase and amplitude of each matrix element. Figure 5.13 (b) shows the output intensities of 3069 iterations with a relative background offset of 0.001 on each measurement. The input amplitude on each segment is 1.

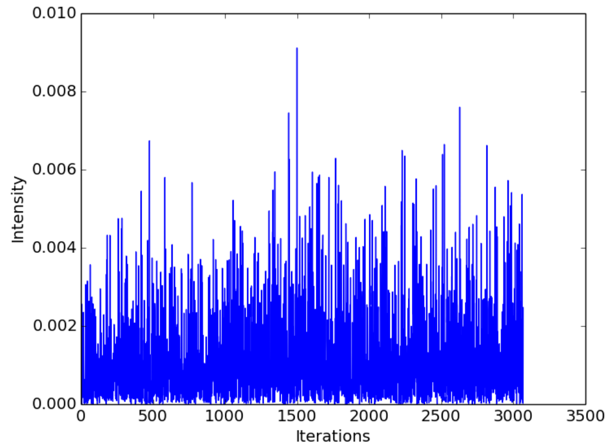

(a)

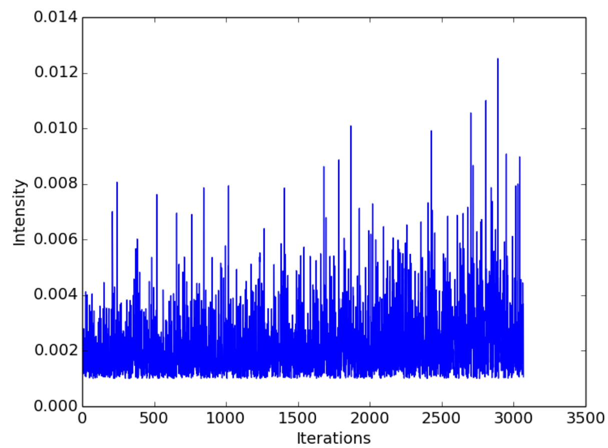

(b)

Figure 5.13: Output intensities of the 3069 measurements. (a) Without background. (b) With background offset of 0.001.

Figure 5.14 shows the calculated values $\cos(\Delta\varphi)$ (eq. 4.24). The blue curve represents the values of the second step ($\Delta\varphi = \varphi_m^2 - \varphi_m^n$) (eq. 4.23), and the green curve represents the values of the third step ($\Delta\varphi = \varphi_m^{2'} - \varphi_m^{n'}$) (eq. 4. 24). The absolute difference of these two curves is used to resolve the sign ambiguity in the calculation of φ_m^n . Figure 5.14(a) shows the results without the measurement offset and Figure 5.14(b) shows the result with the offset. The offset results in calculated values of $\Delta\varphi$ higher than the actual value so that it is always larger than the small value δ of 0.1.

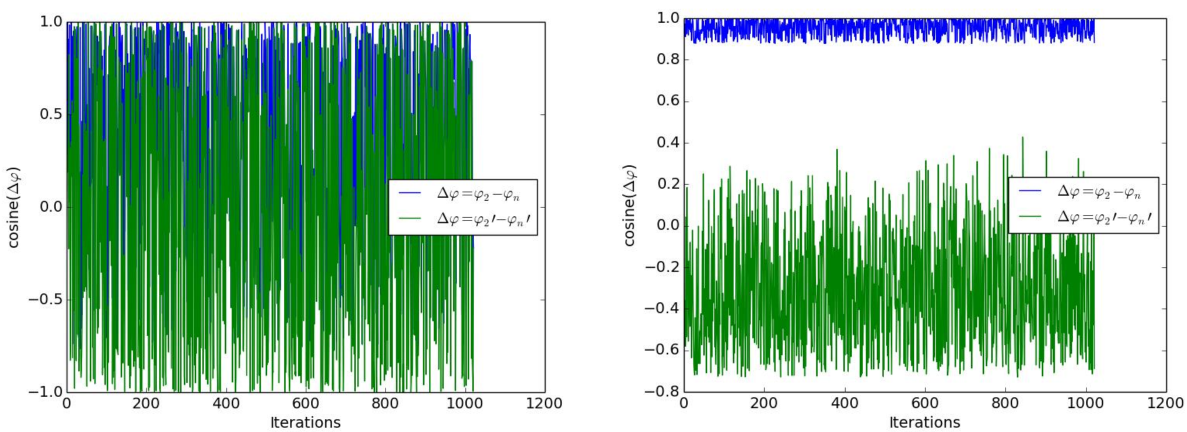

(a) (b)

Figure 5.14: The value $\cos(\Delta\varphi)$ at the second (blue) and third (green) step. (a) Without background. (b) With background of 0.001.

Figure 5.15 shows the phase φ_m^n on each segment before (blue) and after (green) being checked on the third step. The test without noise shows that the phases before being checked have a mean value of $\frac{\pi}{2} \approx 1.57$, Figure 5.15(a). And some phases are changed to $-\varphi_m^n$, with a new mean value of 0.03. The new phases are compared with $\frac{\pi}{2}$ to determine the binary mask on each segment, Figure 5.16(a). Finally, the corrected image with an enhancement of 166 is shown in Figure 5.16(b).

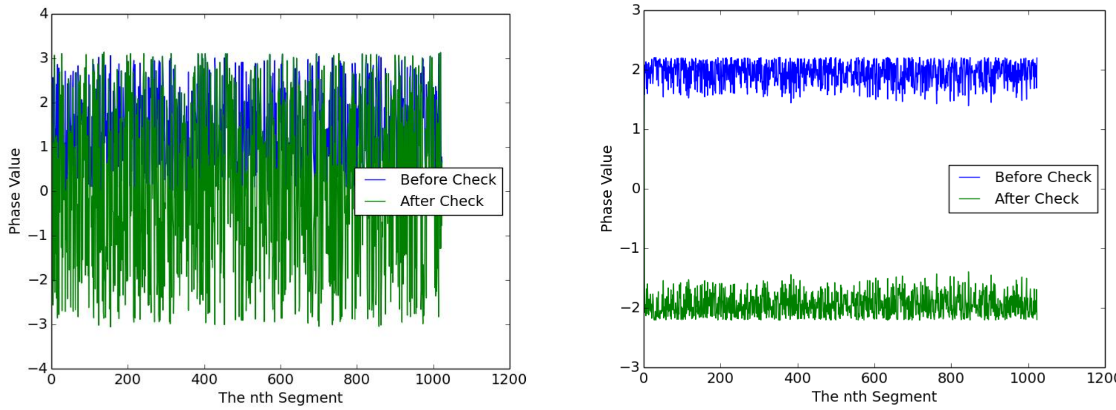

(a) (b)

Figure 5.15: Phase value on each segment. (a) Phases under test without offset. (b) Phases under test with offset.

However, the test with a background shows that all the phases take on the negative value, and the two curves have mean values of 1.94 and -1.94. In this case, if we continue to compare the new phases with $\frac{\pi}{2}$ to determine the binary mask, there would be a huge error. The resulting binary mask and optimized image with an enhancement of 4.5 (much lower than 166) are show in Figure 5.17(a)-(b). The result does not agree with theoretical simulation. If, instead, we compare the new phases with their mean value of -1.94 to determine the binary mask, Figure 5.18(a), the enhancement after optimization is 136, which is very close to the theoretical value of

166, Figure 5.18(b). This illustrates that in real experiments with background, one needs to subtract the background from the CCD camera measurements and compare the new phases with their mean value in order to achieve a better optimization. If the background is not subtracted, $\cos(\Delta\varphi)$ (eq. 4.24) is not in the range -1 to 1 and $\Delta\varphi$ is not a number.

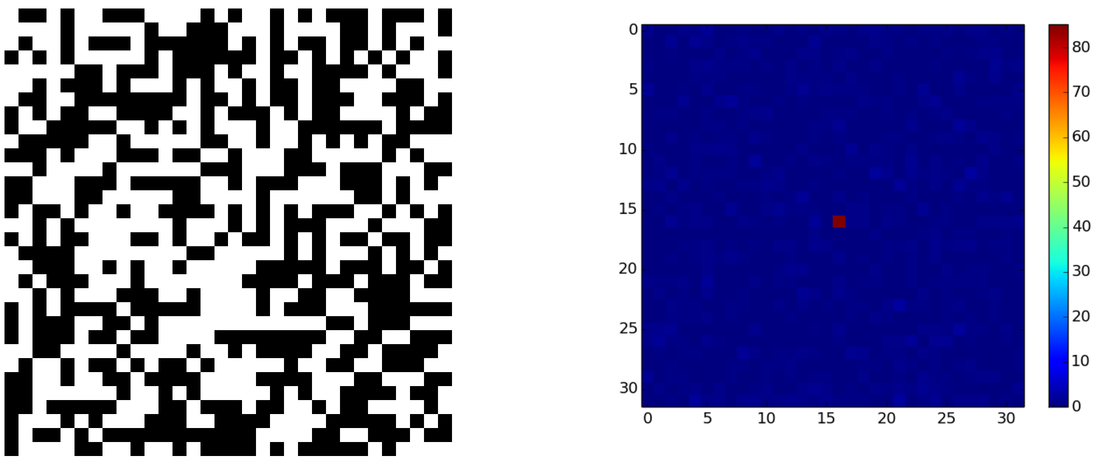

(a) (b)

Figure 5.16. (a) The resulting Binary mask on DMD from the simulation without background. It is determined by comparing new phases with $\frac{\pi}{2}$ as in Equation 4.23. (b) The resulting Optimized image with an enhancement of 166.

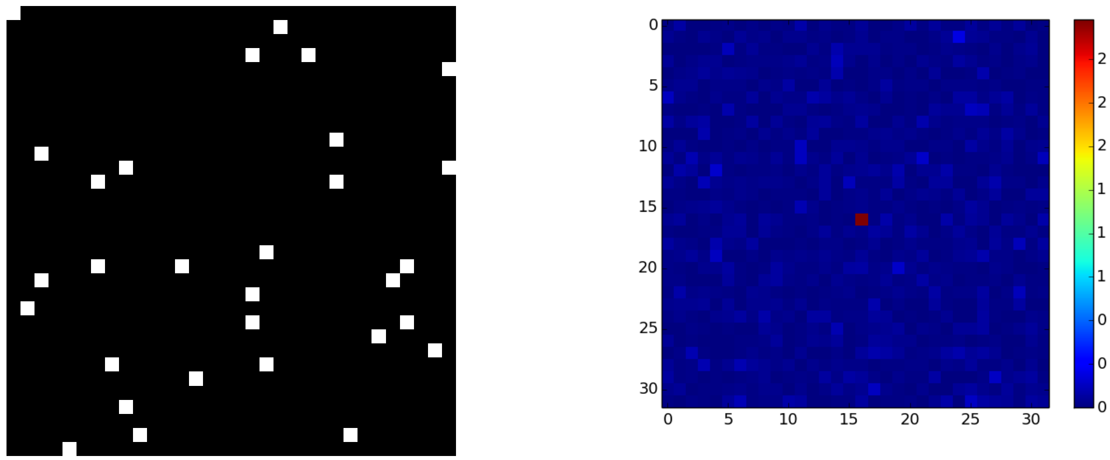

(a) (b)

Figure 5.17: (a) The resulting Binary mask on the DMD of from the simulation with background. Again, the mask is determined by comparing the new phases with $\frac{\pi}{2}$. (b) The Optimized image with an enhancement of 4.5.

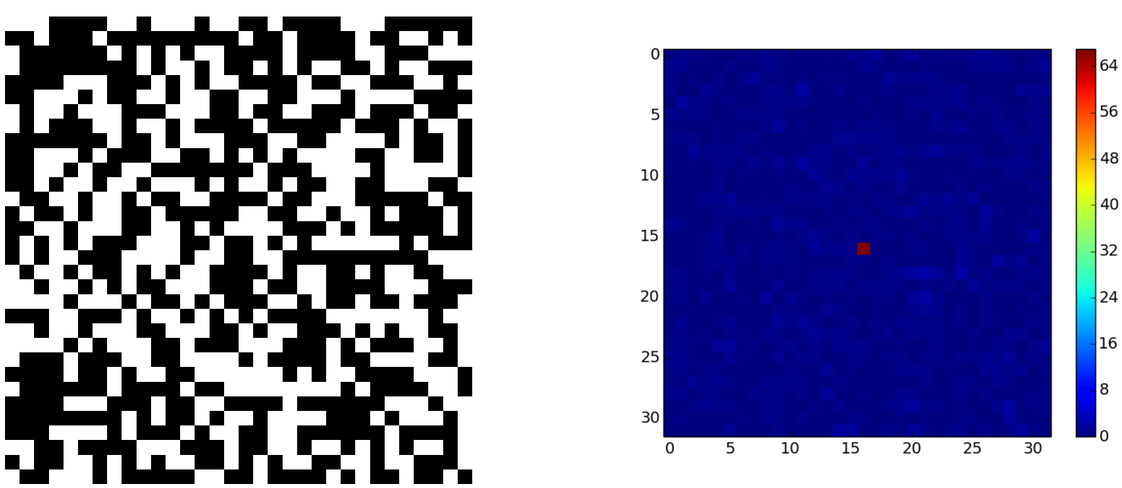

(a) (b)

Figure 5.18: (a) The Binary mask on the DMD of the simulation with background. It is determined by comparing the new phases with their mean value of -1.94. (b) The Optimized image with an enhancement of 136.

5.8 Experimental Results of the Binary Transmission Matrix Algorithm

5.8.1 Experiments with DMD

The Transmission Matrix algorithm is applied to measurements on both the DMD and the SLM, and we achieve good optimization with both devices. On the DMD we made measurements with N= 384, 1536 and 6144 segments. The phases for each experiment are shown in Figure 5.19(a), (c) and (e). We can see that the phases before the check and after the check are shifted to two sides around their mean values, which is similar to the simulation with background. This means that the experimental intensity measurements still contain an error even though we have performed a background subtraction on the output intensity. But, after comparing the new phases with their mean values, a bright focus can be created at the image, Figure 5.19(b), (d) and (e). The enhancements are 43, 136 and 536 respectively for 384, 1536, and 6144 segments, and the enhancement is proportional to the number of segments N and agrees with the theory, Figure 5.20.

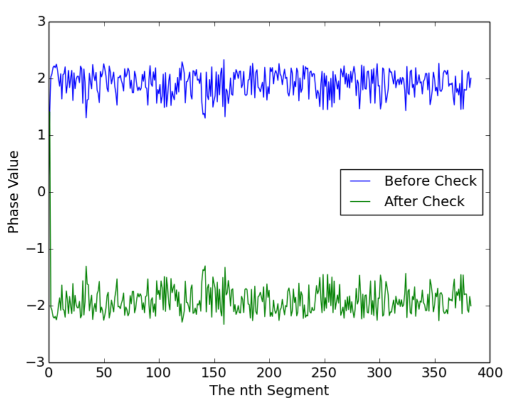

(a)

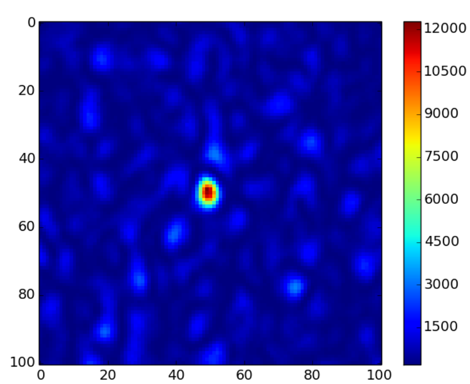

(b)

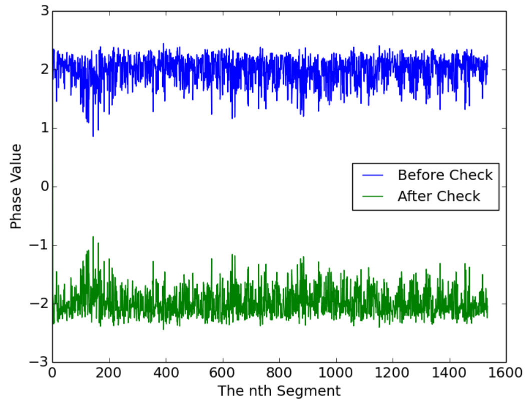

(c)

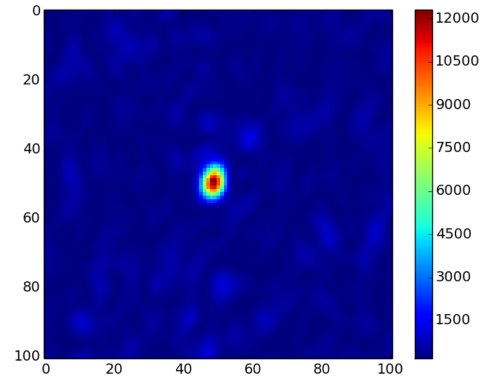

(d)

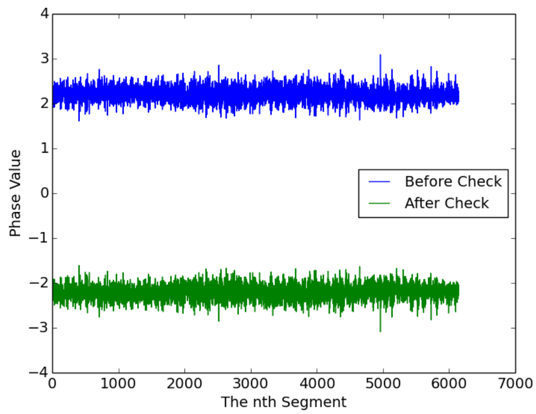

(e)

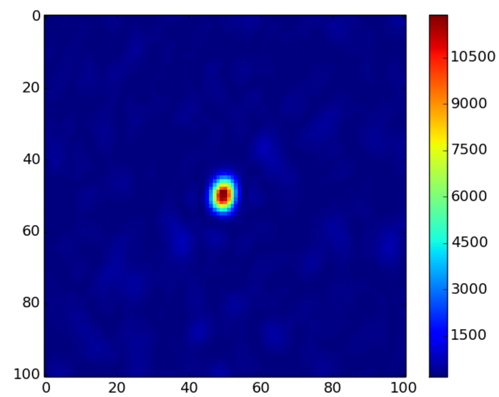

(f)

Figure 5.19: Experimental results with the DMD. (a), (c), (e) show the phases on the DMD with N=384, 1536, 6144, respectively. (b), (d), (f) show the images after binary wavefront optimization with N=384, 1536, 6144, respectively.

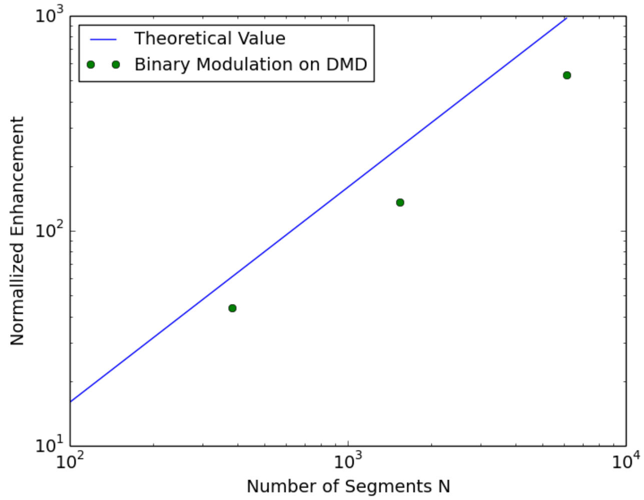

Figure 5.20: A comparison of experimental results on DMD with theoretical value.

5.8.2 Experiment with SLM

Experimental results performed on the SLM are displayed in Figure 5-21. We made measurements with N=256, 1536 and 4096 segments. The achieved enhancements are 40, 123 and 358 respectively which are compared with the theoretical curve in Figure 5-22.

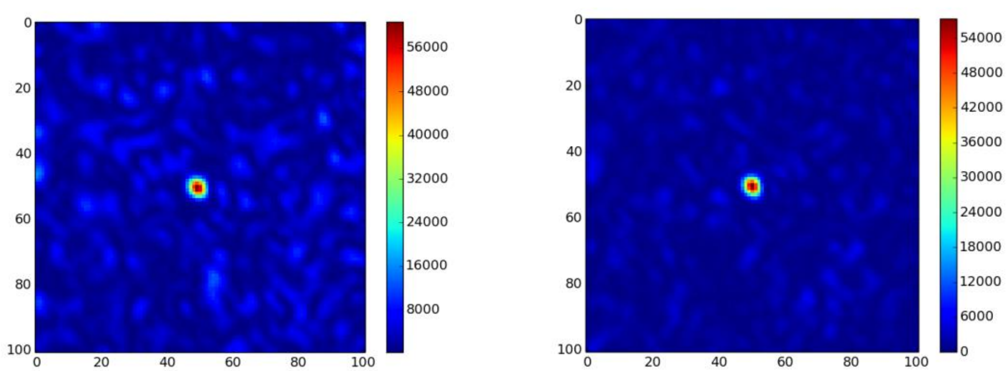

(a) (b)

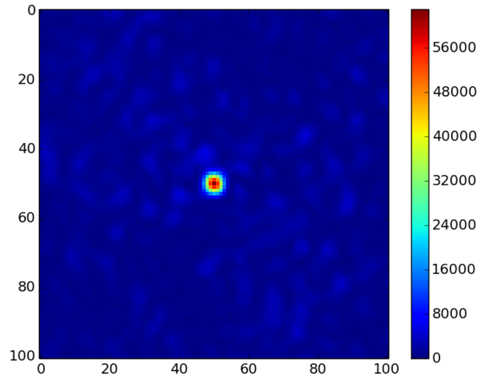

(c)

Figure 5.21: Optimized image with SLM. (a) Enhancement is 40 with N=256. (b) Enhancement is 123 with N=1024. (a) Enhancement is 358 with N=4096.

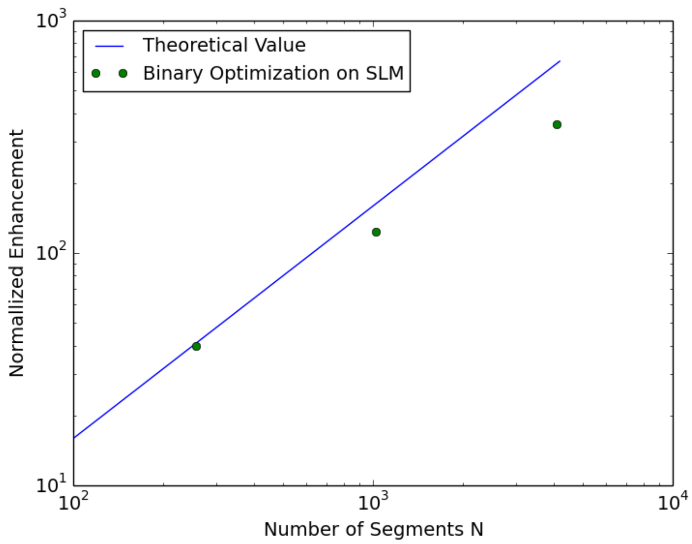

Figure 5.22: A comparison of experimental results on SLM with theoretical value ($\eta = N/2\pi$).

A comparison of our experimental results and other groups' are shown in Table 5.1.

Table 5.1 A comparison of experimental results

Binary Algorithm	N	Enhancement	e/N
GA(DMD)	3072	117	3.81%
GA(SLM)	1024	105	10.25%
TM(DMD)	6144	536	8.72%
TM(SLM)	1024	123	12.01%
Mosk(DMD)	3228	19	0.6%
Mosk(SLM)	800	75	9.38%
Choi(DMD)	10,000	343	3.43%

CHAPTER 6

CONCLUSIONS

We have demonstrated that binary wavefront optimization can successfully and effectively be used to focus light through turbid media. We have developed two new algorithms, a genetic algorithm and a transmission matrix algorithm, which can adaptively find the optimum binary wavefront with enhancements higher than that found using other algorithms such as the binary stepwise method.

Binary wavefront optimization will produce an enhancement $\pi^2/2 \cong 4.9$ lower than phase wavefront optimization, but the DMD is more than five times faster than an SLM so more segments can be used and a higher enhancement should be possible in the same amount of time. The experimental enhancement measured using binary wavefront modulation has so far been significantly lower than the theoretical value.

For the genetic algorithm, we have measured an enhancement of e=117 with N=3072 segments (e/N~3.81%) using a DMD and 105 with 1024 segments using a SLM (e/N~10.25%). And for transmission matrix algorithm, we have measured an enhancement of e=532 with N=6144 segments (e/N~8.66%) using a DMD and 358 with 4096 segments using a SLM (e/N~8.74%). Akbulut et al. have measured an enhancement of 19 with 3228 segments using a DMD (e/N~0.6%) and 75 with 800 segments using an SLM (e/N~9.38%) [9]. Kim et al. have measured an enhancement of 343 with N=10,000 segments (e/N~3.43%) focusing light through a multimode fiber using a DMD [33]. It is an interesting question why the enhancement is consistently much lower than the theory predicts (e/n~15.9%) for the DMD although the literature dose show a range of enhancement factors for different measurements [4] Here we have demonstrated the highest enhancement with a DMD using the transmission matrix algorithm.

Future work will focus on achieving enhancements close to the theoretical limit and applying the approach to different materials. Increasing the speed of the measurements is also an important goal for wavefront optimization so that the techniques can be applied to materials with shorter persistence times. The measurement speed is limited by several reasons such as the DMD switching rate and the CCD frame rate. Although we have achieved very good results with the transmission matrix algorithm, the background subtraction is still not effective, as can be seen from the narrow band of calculated phases; the phases should be more evenly distributed between 0 and 2π We will continue to work on effective methods for subtracting the correct background value from each intensity measurement. For example, because of diffraction, some residual light from other orders can also propagate to the -1 order, becoming background noise on the camera. In this case, we can use a mask to block it so that the light cannot be imaged on the CCD.

In summary, this study accomplished the first use of a genetic algorithm and an intensity only transmission matrix algorithm with binary amplitude modulation. We achieved very good results compared with previous work on binary amplitude modulation.

BIBLIOGRAPHY

1. http://www.nih.gov/science/brain/ (accessed Jun 28, 2014).
2. Tang, J., R.N. Germain, and M. Cui, Superpenetration optical microscopy by iterative multiphoton adaptive compensation technique. Proceedings of the National Academy of Sciences, 2012.
3. http://best-weightlossshakes.com/best-diet-shakes/ whole-milk-helps-in-weight-loss.html (accessed Jun 7, 2012).
4. Vellekoop, I.M. and A.P. Mosk, Focusing coherent light through opaque strongly scattering media. Optics Letters, 2007. 32(16): p. 2309-2311.
5. Vellekoop, I.M. and A.P. Mosk, Phase control algorithms for focusing light through turbid media. Optics Communications, 2008. 281(11): p. 3071-3080.
6. Cui, M., Parallel wavefront optimization method for focusing light through random scattering media. Opt. Lett., 2011. 36(6): p. 870-872.
7. Conkey, D.B., et al., Genetic algorithm optimization for focusing through turbid media in noisy environments. Opt. Express, 2012. 20(5): p. 4840-4849.
8. Popoff, S.M., et al., Measuring the Transmission Matrix in Optics: An Approach to the Study and Control of Light Propagation in Disordered Media. Physical Review Letters, 2010. 104(10): p. 100601.
9. Akbulut, D., et al., Focusing light through random photonic media by binary amplitude modulation. Optics Express, 2011. 19(5): p. 4017-4029.
10. Conkey, D.B., A.M. Caravaca-Aguirre, and R. Piestun, High-speed scattering medium characterization with application to focusing light through turbid media. Opt. Express, 2012. 20(2): p. 1733-1740.
11. Kim, D., et al. Pixelation-free and real-time endoscopic imaging through a fiber bundle. ArXiv e-prints, 2013. 1308, 1308.6719.
12. http://en.wikipedia.org/wiki/Scattering (accessed Jun 20, 2014).
13. Tuchin, V.V., Tissue Optics: Light Scattering Methods and Instruments for Medical Diagnosis. 2007, Bellingham, WA: SPIE Press.
14. Huas, H.A., Waves and Fields in Optoelectronics. 1984, Englewood Cliffs, N.J.: Prentice-Hall, Inc.
15. Van Putten, E.G., I.M. Vellekoop, and A.P. Mosk, Spatial amplitude and phase modulation using commercial twisted nematic LCDs. Applied Optics, 2008. 47(12): p. 2076-2081.

16. http://lyot.org/background/adaptive_optics.html (accessed Jun 2, 2014).
17. Hardy, J.W., Adaptive Optics for Astronomical Telescopes. 1998, New York, N.Y.: Oxford University Press.
18. http://www.npr.org/2013/06/24/190986008/ for-sharpest-views-scope-the-sky-with-quick-change-mirrors (accessed Jun 7, 2014).
19. http://en.wikipedia.org/wiki/Shack_Hartmann_wavefront_sensor (accessed Jun 28, 2014).
20. Booth, M.J., et al., Adaptive aberration correction in a confocal microscope. Proceedings of the National Academy of Sciences, 2002. 99(9): p. 5788-5792.
21. Wright, A.J., et al., Exploration of the optimisation algorithms used in the implementation of adaptive optics in confocal and multiphoton microscopy. Microscopy Research and Technique, 2005. 67(1): p. 36-44.
22. Sherman, L., et al., Adaptive correction of depth-induced aberrations in multiphoton scanning microscopy using a deformable mirror. Journal of Microscopy, 2002. 206(1): p. 65-71.
23. Marsh, P., D. Burns, and J. Girkin, Practical implementation of adaptive optics in multiphoton microscopy. Optics Express, 2003. 11(10): p. 1123-1130.
24. Theofanidou, E., et al., Spherical aberration correction for optical tweezers. Optics Communications, 2004. 236(1–3): p. 145-150.
25. Booth, M., Wave front sensor-less adaptive optics: a model-based approach using sphere packings. Optics Express, 2006. 14(4): p. 1339-1352.
26. Kubby, J.A., Adptive Optics for Biogical Imaging. 2013, Boca Raton, F.L.: CRC Press.
27. Tyson, R.K., Principles of Adaptive Optics. 1997, San Diego, G.A.: ACADEMIC Press.
28. http://laser.physics.sunysb.edu/~melia/SLM_intro.html (accessed Jun 4, 2014).
29. http://bnonlinear.com/pdf/XYSeriesDS0909.pdf - page=11 (accessed Jun 4, 2014).
30. http://www.coretronic.com/en/products02.php (accessed Jun 5, 2014).
31. http://www.ti.com/lit/an/dlpa008/dlpa008.pdf (accessed Jun 22, 2014).
32. http://omlc.org/calc/mie_calc.html (accessed Jun 28, 2014).
33. Kim, D., et al., Pixelation-free and real-time endoscopic imaging through a fiber bundle. arXiv preprint arXiv:1308.6719, 2013.
34. Birch, P.M., et al., Two-pixel computer-generated hologram with a zero-twist nematic liquid-crystal spatial light modulator. Optics Letters, 2000. 25(14): p. 1013-1015.
35. Koza, J.R., Genetic programming: on the programming of computers by means of natural selection. 1992: MIT Press. 680.
36. Choi, Y., et al., Overcoming the Diffraction Limit Using Multiple Light Scattering in a Highly Disordered Medium. Physical Review Letters, 2011. 107(2): p. 023902.

APPENDIX

A. SIMULATION CODES

Appendix A shows the simulation codes of three modulation methods. A.1 contains the code of ideal phase modulation. A.2 shows the code of Genetic Algorithm using a binary amplitude modulation. And A.3 displays the code of Transmission Matrix Algorithm using a binary amplitude modulation. These programs are written in python.

A.1 Phase modulation code (Ideal Simulation)

```
import Utility as U
import numpy as N
import numpy.random as rd

def randU(Nm):
        Are = rd.randn(Nm,Nm)
        Aim = rd.randn(Nm,Nm)
        A = Are + 1j*Aim
        Q,R = N.linalg.qr(A)
        B = N.dot(Q,N.diag(N.diag(R)/N.diag(abs(R))))
        return B

def setphase(p,phi):
        p = N.abs(p)*N.exp(1j*phi)
        return p

def prop_c_2(Nx=32,Nb=1):
        focus_spot = 16.5*32
        T = randU(Nx**2)
        Ei = N.ones((Nx,Nx), dtype=N.complex64)
```

```
    Ei = Ei/N.sqrt(abs(Ei.sum()))
    Eif = Ei.reshape((Nx**2,1))
    no_blocks = Nx**2/Nb
    for m in range(no_blocks):
        phi = N.angle(T[focus_spot,(m*Nb):((m+1)*Nb)].sum())
        for k in range((m*Nb),((m+1)*Nb)):
            Eif[k] = setphase(Eif[k],-phi)
    Eof = N.dot(T,Eif)
    Ei = Eif.reshape((Nx,Nx))
    Eo = Eof.reshape((Nx,Nx))
    im = abs(eod)**2)
    return (Ei,Eo,im)
```

A.2 Binary amplitude modulation code (Genetic Algorithm Simulation)

```
def randU(Nm):
    Are = N.random.randn(Nm,Nm)
    Aim = N.random.randn(Nm,Nm)
    A = Are + 1j*Aim
    Q,R = N.linalg.qr(A)
    B = N.dot(Q,N.diag(N.diag(R)/N.diag(abs(R))))
    # Note N.transpose does not take complex conjugate
    return B

def parents(R,C,n):
    pt = N.zeros((n,R,C),dtype=N.float32)
    for i in range(n):
        fm = N.random.randint(2,size=R*C)
        pt[i] = fm.reshape(R,C)
    return pt

def rankpt(TM,R,C,n):
    pt = parents(R,C,n)
    Ints = N.zeros((n),dtype=N.float32)
    newpt = N.zeros((n,R,C),dtype=N.float32)
    newptInts = N.zeros((n),dtype=N.float32)
```

```
    focus_spot = R*C/2.0+N.sqrt(R*C)/2
    for i in range(n):
        Ints[i] = N.abs(N.dot(TM[focus_spot,:],pt[i].reshape((R*C,1))))**2
    newptInts = N.array(Ints)
    newptInts.sort()
    for j in range(n):
        newpt[j] = pt[Ints.tolist().index(newptInts[j])]
    return (newpt,newptInts)

def tempulate(R,C):
    t = N.random.randint(2,size=R*C)
    T = t.reshape(R,C)
    return T

def breed(TM,pt,ptInts,R,C,n,j):#generate G=N/2 offspring
    offsp = N.zeros((n/2,R,C),dtype=N.float32)
    newpt = N.zeros((n,R,C),dtype=N.float32)
    Ints = N.zeros((n/2),dtype=N.float32)
    newptInts = N.zeros((n),dtype=N.float32)
    number = N.arange(n)
    partition = N.cumsum(number)
    T = tempulate(R,C)
    focus_spot = R*C/2.0+N.sqrt(R*C)/2

    for i in range(1,(n/2+1)):
        ma = mp(partition,n)
        ma = pt[ma]
        pa = mp(partition,n)
        pa = pt[pa]
        offspring = ma*T + pa*(1-T)#randomly choose x segment from mother and R*C-x
segments from father.
        mutation = mutate(R,C,j,offspring)
        offsp[i-1] = mutation
        Ints[i-1] = N.abs(N.dot(TM[focus_spot,:],mutation.reshape((R*C,1))))**2
    pt[0:n/2] = offsp[:]
    ptInts[0:n/2] = Ints[:]
    newptInts = N.array(ptInts)
    newptInts.sort()
    for j in range(n):
```

```
        newpt[j] = pt[ptInts.tolist().index(newptInts[j])]
    return (newpt,newptInts)

def mp(partition,n):
    p = partition[n-1]*N.random.rand()
    choice = partition.searchsorted(p)
    return choice

def mutate(R,C,numb,offspring):
    R0 = 0.01
    Rend = 0.0025
    factor = 650.0
    RR = (R0-Rend)*N.exp(-numb/factor) + Rend
    for j in range(N.int(R*C*RR)):#RR percentage of the total segments would be mutated.
        m = N.random.randint(0,R)
        n = N.random.randint(0,C)
        val = offspring[m,n]
        if (val== 0):
            offspring[m,n] = 1
        else:
            offspring[m,n] = 0
    return offspring

def genetic(pt,ptInts,R,C,m):# try R=32,C=32
    start = time.time()
    TM = randU(R*C)
    focus_spot = R*C/2.0+N.sqrt(R*C)/2
    before = parents(R,C,1)
    before = before[0].reshape((R*C,1))
    Imz = N.abs(N.dot(TM,before))**2
    Intsz = Imz.mean()
    Ehc = N.zeros((1,m),dtype=N.float32)
    fmask = N.zeros((m,R,C))# save final best mask of each iteration
    gints = N.zeros((m,R,C))# save final intensity of each iteration

    for n in range(50,60,20):
        for i in range(0,m):
            pt,ptInts = breed(TM,pt,ptInts,R,C,n,i)#generate G=N/2 offspring
            fmask[i] = pt[n-1]
```

```
            gints[i] = (N.abs(N.dot(TM,pt[n-1].reshape((R*C,1))))**2).reshape(R,C)
            Ints = ptInts[n-1]
            Ehc[(n/5-10),i] = float(Ints)/float(Intsz)
    end = time.time()
    lens = (end - start)/60.0
    x = range(m)
    plt.figure()
    plt.plot(x,Ehc[0])
    plt.legend(('Population=50',), loc = 'lower right')
    plt.xlabel('Generation')
    plt.ylabel('Enhancement')
    print lens
    print Ehc.max()
    return (Ehc,fmask,gints)
```

A.3 Binary amplitude modulation code (Transmission Matrix Algorithm Simulation)

```
def randU(Nm):
    Are = N.random.randn(Nm,Nm)
    Aim = N.random.randn(Nm,Nm)
    A = Are + 1j*Aim
    Q,R = N.linalg.qr(A)
    B = N.dot(Q,N.diag(N.diag(R)/N.diag(abs(R))))
    return B

def getTM_b(Nx=4):
    ''' calculate the transfer matrix by measuring pairs of terms try one row,
        now with hadamard matrix to even out intensity '''
    T = randU(Nx)
    H = 0.5*(hadamard(Nx)+1)
    Tr = T[0,:]
    # generate measurement matrix
    M = N.zeros((Nx,3*Nx-3))
    for m in range(Nx):
        # first Nx columns
        M[m,m] = 1
```

```
        # second Nx columns
        if m<(Nx-1):
                M[0,Nx+m] = 1
                M[m+1,Nx+m] = 1
        # 3rd set of columns
        if m<(Nx-2):
                M[1,2*Nx+m-1] = 1
                M[m+2,2*Nx+m-1] = 1
# get measurements
out = abs(N.dot(Tr,M))**2
# decode
phis = N.zeros(Nx)
amps = N.zeros(Nx)
amps = N.sqrt(out[:Nx])
for m in range(Nx-1):
        a = out[0]
        b = out[m+1]
        s = out[Nx+m]
        phis[m+1] = N.arccos((s-a-b)/N.sqrt(a*b)/2)
print phis
# sign check
for m in range(Nx-2):
        a = out[1]
        b = out[m+2]
        s = out[2*Nx-1+m]
        ctwo = (s-a-b)/N.sqrt(a*b)/2
        cphi = N.cos(phis[1]-phis[m+2])
        if abs(ctwo-cphi)>0.1:
                phis[m+2] = - phis[m+2]
q = N.angle(Tr)-N.angle(Tr)[0]
print phis
print q
print amps
print abs(Tr)
return (H,M)
```